

# Sensorless Control of a Hybrid Stepper Motor

**Lina Karlsson**

Master of Science Thesis in Electrical Engineering  
**Sensorless Control of a Hybrid Stepper Motor**

Lina Karlsson

LiTH-ISY-EX--16/4962--SE

Supervisor: **Sergii Voronov**  
ISY, Linköping University  
**Stefan Grufman**  
Husqvarna AB

Examiner: **Mattias Krylander**  
ISY, Linköping University

*Division of Automatic Control  
Department of Electrical Engineering  
Linköping University  
SE-581 83 Linköping, Sweden*

Copyright © 2016 Lina Karlsson

## Abstract

Electrical drives are widely used in today's society. They can be found in both household products and in the industry. One application where electrical drives are used is in robots for mowing lawns. In the studied robots the motors in the electrical drives used for propulsion are Brush Less Direct Current motors, BLDC-motors. The BLDC-motor has its maximum torque at high speeds and therefore a gearbox is needed. The gearbox is space consuming, add costs and consists of mechanical parts that wear during use. Of interest is therefore to investigate if there are other electrical drives which can be used for propulsion.

A motor who has its maximum torque at low speeds is the Stepper motor, and therefore it is of interest to investigate if a stepper motor could replace the BLDC-motor. A drawback with the stepper motor is that it always consumes maximum current and therefore a current controller is beneficial. Together with current control, speed control is needed to make the robot run at desired speed. To be able to perform an accurate current and speed control feedback from the motor is needed. Information about the rotor angle and velocity can be used for the speed control and the load angle can be used for the current control since the current is proportional to the load torque.

To estimate the rotor angle and velocity a model has been developed. The model is based on fundamental electrical and mechanical equations and neglects the current and position dependence of the inductance and flux linkage. To complete the model three motor parameters, the maximum detent torque  $T_{dm}$ , the maximum flux linkage  $\psi_m$  and the friction constant  $B$  was determined. Parameter determination was done by linear regression and by using an Extended Kalman Filter, EKF. The result of the parameter determination were  $T_{dm} = 0.2152$  Nm,  $\psi_m = -0.002854$  Vs/rad and  $B = 0.01186$  Nms/rad.

The model is used in an EKF to estimate the rotor angle and angular velocity. The result of the implemented EKF seems promising. When making the rotor take a step in velocity from 3.927 rad/s to 7.85 rad/s the EKF estimates the states with only a small bias: 0.02 rad for the angle, 0.3 rad/s for the velocity, 0.005 A for phase a current and 0.0004 A for phase b current.

To estimate the load angle the Sliding Discrete Fourier Transform is used. The expected relation between the load torque and load angle is sinusoidal. The load angle is calculated from data where the external load is between 0-2.5 Nm. In that area the load angle shows the expected sinusoidal appearance and the load angle is in the area between 0.1 and 0.45 rad. At 3 Nm the rotor stalls and it is shown that the load angle varies between 0 and  $2\pi$  rad when the rotor is stalled.



## Acknowledgments

First of all, I want to begin by thanking Husqvarna AB for providing me with the opportunity to perform this master's thesis work. I want to show my gratitude to all who have supported me. Especially thanks to Magnus Öhrlund for introducing me to the project and describing potentials of stepper motors, Pär-Ola Svensson for your support with the equipment, Martin Larsén for sharing your knowledge about motors, Jonas Rangsjö for your help with the EKF, and finally Stefan Grufman for organizing everything.

I also want to express my gratitude to my examiner Mattias Krylander and supervisor Sergii Voronov. They have always been available for discussions regarding the motor model, estimation methods and implementation problems.

Finally, I want to thank my family for helping me through seventeen years of studies, and my fiancé, Mattias Lindbäck, for encouraging me and always believing in me.

*Linköping, June 2016*  
*Lina Karlsson*



---

# Contents

<b>Notation</b>	<b>ix</b>
<b>1 Introduction</b>	<b>1</b>
1.1 Motivation . . . . .	2
1.2 Problem formulation . . . . .	2
1.3 Outline . . . . .	3
<b>2 Related work</b>	<b>5</b>
<b>3 Theoretical background</b>	<b>7</b>
3.1 Hybrid Stepper Motor . . . . .	7
3.2 Load Angle . . . . .	9
3.3 Sliding Discrete Fourier Transform . . . . .	11
3.4 Multiple linear regression . . . . .	12
3.5 Residual analysis . . . . .	12
3.6 Extended Kalman Filter . . . . .	13
<b>4 Data collection</b>	<b>15</b>
4.1 Equipment setup . . . . .	15
4.2 Collected Data . . . . .	17
<b>5 Modeling</b>	<b>23</b>
5.1 Motor model . . . . .	23
<b>6 Determination of unknown motor parameters</b>	<b>27</b>
6.1 Determination of parameters individually . . . . .	27
6.1.1 Detent torque . . . . .	27
6.1.2 Friction constant . . . . .	27
6.1.3 Maximum flux linkage . . . . .	30
6.2 Determination with multiple linear regression . . . . .	32
6.3 Determination with the Extended Kalman Filter . . . . .	34
6.3.1 Choose filter parameters . . . . .	37
6.4 Residual analysis . . . . .	39

---

<b>7</b>	<b>Estimations</b>	<b>45</b>
7.1	Extended Kalman Filter . . . . .	45
7.2	Load angle estimation . . . . .	46
<b>8</b>	<b>Results</b>	<b>49</b>
8.1	Evaluation of model and model parameters . . . . .	49
8.2	Evaluation of the EKF . . . . .	50
8.3	Evaluation of load angle estimations . . . . .	51
<b>9</b>	<b>Discussion</b>	<b>59</b>
9.1	Results . . . . .	59
9.1.1	Motor model and parameters . . . . .	59
9.1.2	EKF and load angle . . . . .	60
9.2	Future work . . . . .	61
9.2.1	Parameter determination . . . . .	61
9.2.2	Extended Kalman Filter . . . . .	62
9.2.3	Load angle . . . . .	62
<b>10</b>	<b>Conclusions</b>	<b>63</b>
	<b>Bibliography</b>	<b>65</b>

---

# Notation

## ACRONYMS

Acronym	Meaning
ACF	Autocorrelation Function
BLDC	Brush Less Direct Current
DFT	Discrete Fourier Transform
EKF	Extended Kalman Filter
EMF	Electromotive Force
HSM	Hybrid Stepper Motor
ODE	Ordinary Differential Equation
OLS	Ordinary Least Squares
RSS	Residual Sum of Squares
SDTF	Sliding Discrete Fourier Transform

## SYMBOLS

Symbol	Meaning
$L$	inductance [H]
$R$	resistance [ $\Omega$ ]
$J$	inertia [ $kgm^2$ ]
$B$	friction coefficient [Nms/rad]
$e_j$	back electromotive force for phase j [Vs]
$\psi$	flux linkage [Vs/rad]
$\psi_{max}$	maximum flux linkage [Vs/rad]
$\theta$	rotor angle [rad]
$\omega$	rotor angular velocity [rad/s]
$i_j$	phase j current [A]
$v_j$	phase j voltage [V]
$T_j$	torque produced by phase j [Nm]
$T_D$	detent torque [Nm]
$T_L$	load torque [Nm]
$\delta$	load angle [rad]



# 1

## Introduction

Everywhere in today's society, it is possible to come across products whose functionality is based on motion. In most households you probably can find products such as household appliances, tools, watches, fans, hair dryers, printers and toys, and in the industry you can find robots, vehicles, elevators, escalators, rolling mills and pumps. What enables the movement in all these products are electrical drives.

An electrical drive has five main functional blocks: power source, power modulator, motor, mechanical load and a control unit. Sometimes also a sensing unit is added to provide feedback to the control unit, see Figure 1.1.

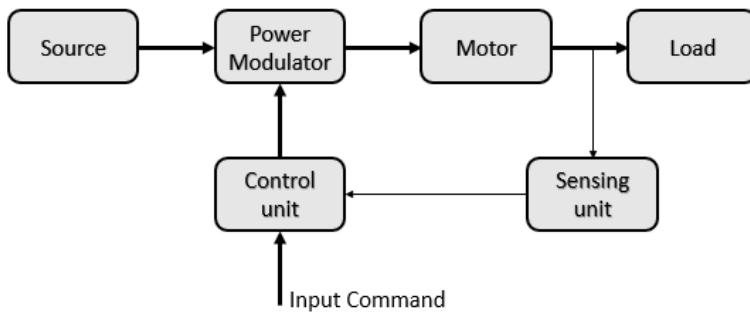


**Figure 1.1:** The main functional blocks of electrical drives.

This master thesis concerns modelling of a Hybrid Stepper Motor (HSM) and developing of a sensorless estimator for the motor. This to develop a basis for a future current and speed controller to an HSM. This first chapter will describe the motivation for this master thesis and why it is an interesting area to investigate. It will also contain the problem formulation and an outline of this thesis report.

## 1.1 Motivation

Husqvarna AB has developed and sold autonomous robots for mowing lawns for 20 years. Important factors are that the robots are energy efficient, not too expensive to manufacture and long lasting without need to repair it.

Today, the motors used for robots propulsion are Brush Less Direct Current motors (BLDC-motor). The BLDC-motor has its maximum torque at a speed above the speed the robot will be run in. Therefore, a gearbox is needed to obtain the desired torque at lower speeds. The disadvantage with this solution is that the gearbox is space consuming, increases the cost of the robot and consists of mechanical parts that wear during use. For that reason it is of interest to investigate if there are other motors that can be used for propulsion without use of a gearbox.

A motor with its maximum torque at low speeds is the stepper motor. The advantage with this motor is thus that a gearbox is not necessary to obtain desired torque at low speeds. A stepper motor is also cheaper than a BLDC-motor. Therefore, introduction of a stepper motor instead of current technology can reduce the cost of the robot, decrease the space of the motor solution and eliminate the problem with worn out gearboxes.

To be able to replace the motor, a new control algorithm needs to be developed. If the load is fixed during drive, a stepper motor can be controlled by an open loop method. However, open loop control often results in torque and speed ripples, noise, vibrations, a poor energy efficiency and no control on step loss. To avoid step loss, motor applications based on open loop control often are driven with maximum current which is not preferable for battery applications.

For applications where the load will vary during drive, a closed loop control is preferred. For closed loop control the most straightforward method is to use a rotor position sensor. A mechanical sensor increase cost and size of the motor and Husqvarna therefore wants a sensorless solution.

## 1.2 Problem formulation

The purpose is to investigate if it is possible to develop a sensorless estimator for a hybrid stepper motor and discuss if the outcome from the estimator can be used to perform a sensorless speed and torque control on a Hybrid Stepper Motor (HSM). To be able to do an accurate speed and torque control of the motor feedback such as rotor angle, rotor velocity and the load angle can be used. The sensorless estimator will use the phase current and phase voltages of the motor to estimate above mentioned states. Due to the lack of hardware, the model and estimator will only be implemented and tested in a simulation environment.

If the result looks promising Husqvarna AB has a basis for further investigation of stepper motors and its potential to replace the BLDC-motors. Further this can decrease the cost of the robot and also increase the lifespan of the motor solution.

## 1.3 Outline

The thesis is organized in several chapters. Chapter 2 shortly describes the related work to this thesis and which kind of solutions that have been used for similar problems. Chapter 3 introduces the background theory of the thesis. In Chapter 4 the equipment for data collection is described. Chapter 5 describes the model of the HSM which will be used in further investigations of the HSM. The model contains of unknown parameters, and how to determine these are described in Chapter 6. In Chapter 7 an Extended Kalman filter is introduced for estimation of the rotor angle and rotor position. In the end of the chapter a method of estimating the load angle is presented. Chapter 8 presents the results of the model and estimator in Matlab. Chapter 9 discusses the result and the future work in this area. Finally, a conclusion is made in Chapter 10.



# 2

---

## Related work

The modern stepping motor was first invented in 1957 by Thomas and Fleischer [10]. Stepping motors are often used in digital control systems where the motor receives open loop commands, in shape of train pulses, to rotate to a specific angle [16]. This makes stepping motors suitable in printers, plotters, CD-players and for tool positioning [16]. But due to the rotor inertia, the rotor oscillates around the goal position before stabilizing which creates an jerky motion of the rotor. Because of this the motor can loose steps if the variation of the load torque is too fast [2]. Usage of programmable architectures like field-programmable gate arrays circuits together with advanced control algorithms enables microstepping of the motors. This makes the rotor motion smoother but problem with step loss still remains [2], [7]. The control algorithms can also optimize the torque dynamics in the motor [7]. To work properly these algorithms needs feedback, such as rotor position or rotor flux, from the motor. This means that a closed loop control needs to be introduced. A closed loop control can be performed either with a positioning sensor or with a rotor position estimator. A position sensor adds costs and complexity, and increase the size of the system. Therefore it is of interest to provide feedback from a positioning estimator instead [7].

A commonly proposed estimator is the Extended Kalman Filter, EKF, which is used to estimate the rotor position and velocity [2], [4], [14]. To be able to implement an EKF a state space model of the motor is needed. Authors in [2], [14] and [15] proposes a model based on fundamental electrical and mechanical equations. The model represents the motor phases separately. According to authors in [2] this is because the Hybrid Stepper Motor has its two phases,  $a$  and  $b$ , in quadrature. The electrical equations neglects the position and current dependence of the permanent magnet flux linkage and inductance. According to authors in [4] this could lead to poor model fit since the significance of the posi-

tion and current dependence may not always be negligible. However, adding this dependence increases the complexity of the model and how much the model fit will increase depends on the available hardware. A decision must also be made if a more complex model is worth an increase in computational costs [4].

The models proposed in [2], [4], [14] and [15] are mostly used for speed and position control and in situations where the load torque is small or varies slowly. In the suggested models the load torque is an unknown source of disturbance and to increase the overall robustness of the system it is useful to also use the EKF to estimate the load torque. To be able to estimate the load torque it is added as a fifth state and an equation explaining the load torque variations is added in the model [14].

To be able to get more information about the load another possibility is to estimate the load angle [5], [6], [7]. The load angle describes the lag between the instantaneous rotor position and the stator current excitation vector and is the angle between the current vector and the vector of the magnetic flux. Since the magnetic flux is perpendicular to the back Electromotive Force (back-EMF) the load angle can be determined by first determine the back EMF [5], [6], [7]. To determine the load angle the authors in [5] proposes a method where the back EMF is determined by sample the voltage at the zero crossing of the current. The authors in [6], [7] instead proposes a method where the back EMF is determined by using the Sliding Discrete Fourier Transform, SDFT.

In this chapter previous work with modelling Hybrid Stepper Motors were presented. Some of the techniques aforementioned will be considered in the thesis to be able to find out if they are applicable in the real world application.

# 3

---

## Theoretical background

This chapter consist of basic knowledge about subjects covered in this thesis. The chapter will first introduce the Hybrid Stepper Motor. It will continue introducing the load angle and the Sliding Discrete Fourier Transform. Next, multiple linear regression, which is a method for estimating parameters to a model equation, is described. The chapter continues by describing residual analysis and how to use it to determine whether a model can explain a data set or not. At last the Extended Kalman Filter is explained.

### 3.1 Hybrid Stepper Motor

Stepping motors are designed to translate switched excitation changes into defined increments of rotor position, so called steps [1]. Stepping motors often produces a large number of steps per revolution, for example 50, 100 or 200 steps per revolution which corresponds to a mechanical rotation of  $7.2^\circ$ ,  $3.6^\circ$  or  $1.8^\circ$  per step [16]. Stepping motors has doubly salient structure, which means that both the rotor and stator teeth consists of magnetically permeable material, see Figure 3.1. As seen in the figure the magnetic flux crosses the air gap between the teeth causing a normal force  $n$ , which tries to close the air gap, and a tangential force  $t$ , which moves the teeth sideways. This forces will be zero as soon as the magnetic flux is removed [1].

The Hybrid Stepper Motor, HSM, has a doubly salient structure [1]. The magnetic circuit is exited by a combination of windings on the stator, and a permanent magnet on the rotor, see Figure 3.2. In the figure the stator poles are wounded separately. It is also possible to wound them together two and two which will improve the torque production [16]. The rotor in a HSM consists of two identical rotor stacks which are displaced axially along the rotor and in angle by one half of the rotor tooth pitch. The rotor tooth pith is the angle between two

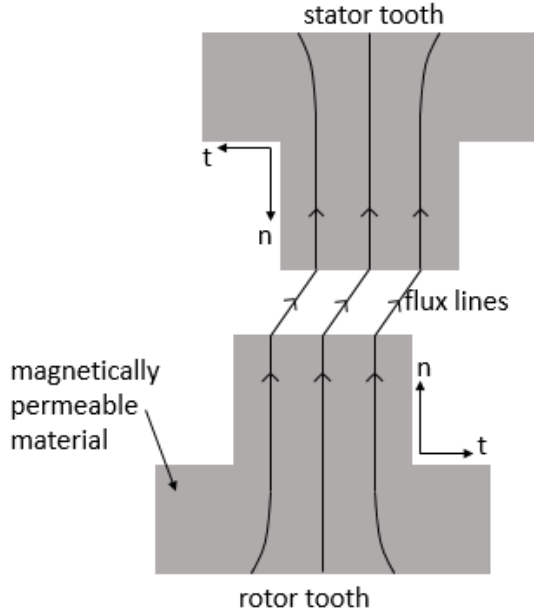


**Figure 3.1:** Rotor and stator teeth in a stepping motor. Vectors  $t$  and  $n$  are the force components between two magnetically permeable teeth.

rotor teeth, see Figure 3.2, and can be calculated as

$$\text{rotor tooth pitch} = \left( \frac{360}{p} \right)^\circ \quad (3.1)$$

where  $p$  is the number of rotor teeth [1]. The HSM has typically eight stator poles which is wound by two phases,  $a$  and  $b$ , see Figure 3.2. Continuous rotation of the motor is provided by exciting the phases  $a$  and  $b$  in desired order. The phases are excited by making current  $i_a$  and  $i_b$  flow through the stator windings. For the HSM illustrated in Figure 3.2 clockwise rotation would be obtained by the excitation sequence  $a+$ ,  $b+$ ,  $a-$ ,  $b-$ ,  $a+$ ,  $b+$ , and so on. Each excitation will make the rotor take one step and a complete cycle of excitation will create four steps. Since the excitation state is the same before and after these four steps the alignment of the stator and rotor teeth will occur under the same stator poles [1]. This means that four steps corresponds to a rotor movement of one rotor tooth pitch and the step length can therefore be related to the number of rotor teeth,  $p$ , as

$$\text{step length} = \left( \frac{90}{p} \right)^\circ.$$

The excitation sequence  $a+$ ,  $b+$ ,  $a-$ ,  $b-$ ,  $a+$ ,  $b+$ ... makes the motor take so called full steps. By excite the phases together, and not only one by one, it is possible to

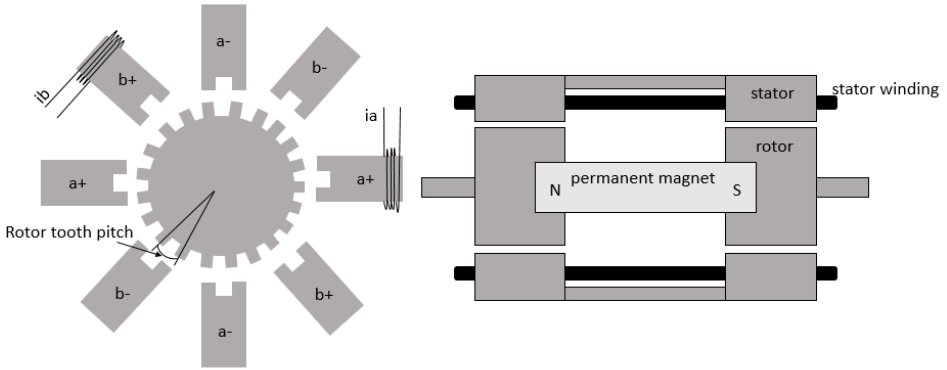


**Figure 3.2:** The left figure shows a cross section of the rotor together with the stator phases a and b. The phases are excited by making current  $i_a$  and  $i_b$  flowing through the stator windings. The right figure shows a side view of an HSM.

make the motor take smaller steps, such as half steps. An illustration of how half steps is created can be seen in Figure 3.3. By using the same principle, together with different current levels it is possible to make the rotor take even smaller steps, so called microsteps.

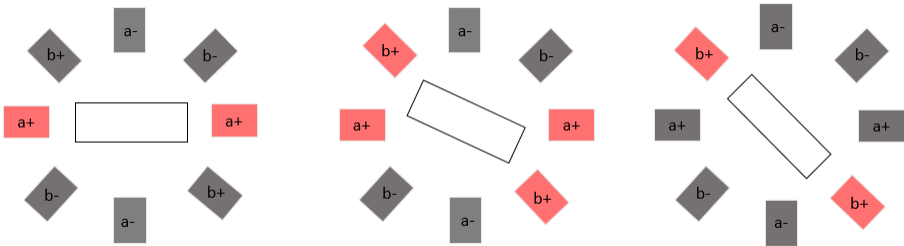


**Figure 3.3:** An illustration of how half step motion is created.

## 3.2 Load Angle

The load angle,  $\delta$ , describes the lag between the instantaneous rotor position and the stator current excitation vector and is the angle between the current vector  $i_s$  and the vector of the permanent magnet rotor flux  $\psi$ , see Figure 3.4. To determine the load angle information about the current vector  $i_s$  and vector of the permanent magnet rotor flux  $\psi$  is needed. Since  $i_s$  is the resulting component of the phase currents  $i_a$  and  $i_b$ , and  $i_a$  and  $i_b$  can be measured, it is possible to determine  $i_s$ . To get information about the permanent magnet rotor flux is not

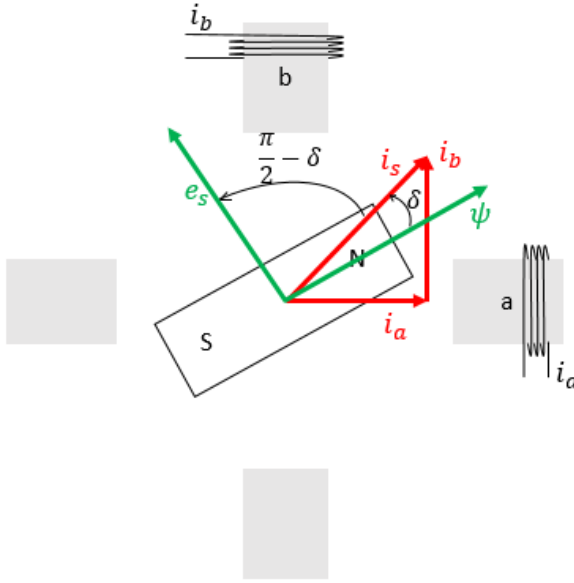


**Figure 3.4:** Current vectors  $i_a$ ,  $i_b$ ,  $i_s$ , flux vector  $\psi_s$ , and back EMF vector  $e_s$  and their relations to the load angle  $\delta$ .

as straightforward. However, by using Lenz's law the back-EMF voltage vector induced by the permanent magnet rotor flux can be written as

$$e_s = C \frac{d\psi}{dt} \quad (3.2)$$

The result of this is a phase lead of  $\pi/2$  rad between the back EMF and the permanent magnet rotor flux vector. From this follows that the angle between the current vector and the back EMF-vector is equal to  $\pi/2 - \delta$ . This means that with knowledge of the current vector  $i_s$  and the back-EMF the load angle can be determined [7].

Of interest is the relation between the load angle and the motor torque. The electromagnetic motor torque vector can be determined with the interaction between the stator flux linkage space vector  $\psi_s$  and the stator current space vector  $i_s$  as

$$T_{motor} = \psi_s \times i_s \quad (3.3)$$

If the saturation is neglected the flux linkage space vector  $\psi_s$  can be written as the sum of the permanent magnet rotor flux  $\psi$  and the stator flux linkages established by the two stator currents. [7]. In the dq-reference frame, which is fixed in the rotor, the motor torque can be written as

$$T_{motor} = (\psi + i_d L_d + i_q L_q) \times i_s \quad (3.4)$$

The electromagnetic torque value can be written as a function of  $i_s$  and the load angle  $\delta$  as

$$T_{motor} = \psi i_s \sin(\delta) + \frac{L_d - L_q}{2} i_s^2 \sin(2\delta) \quad (3.5)$$

In equation (3.5) the first term describes the torque generated by the interaction between  $\psi$  and  $i_s$ . The second term represent the reluctance effect due to the multi toothed rotor. As seen the two terms depend on the sine of the load angle respectively sine of twice the load angle. This means that the relation between the load angle and the generated torque should be sinusoidal. If the motor has two phases the maximum load angle before step loss occurs is  $\pi/2$ .

### 3.3 Sliding Discrete Fourier Transform

To determine the fundamental component of a signal, Fourier analysis can be used [6], [7]. At a discrete time instance  $k$ , the  $h$ th harmonic component  $X_h[k]$  can be written as

$$X_h[k] = \sum_{l=0}^{N-1} x[k - [N - 1] + l] e^{-2\pi h j l / N} \quad (3.6)$$

To be able to calculate the fundamental component,  $h = 1$ , a signal of  $N$  samples is needed. When a new sample is available equation (3.6) updates the fundamental component. To sum all measurement samples over one signal period  $N$  is time consuming. However it is possible to only add the newest sample  $x[n]$  and remove the oldest sample  $x[n-N]$ . This creates a sliding window over the signal in which the fundamental harmonic component is calculated. This operation is called a Sliding Discrete Fourier Transform, SDFT, [6]. The Fourier component  $X_h[k]$  at a time instance  $k$  is written as

$$X_h[k] = x[k - [N - 1]] + x[k - [N - 1] + 1] e^{-2\pi h j / N} + x[k] e^{-2\pi h j [N-1] / N} \quad (3.7)$$

The previous component  $X_h[k - 1]$  is written as

$$X_h[k - 1] = x[k - N] + x[k - [N - 1]] e^{-2\pi h j / N} + x[k - 1] e^{-2\pi h j [N-1] / N} \quad (3.8)$$

Equation (3.8) can also be subtracted from equation (3.7)

$$X_h[k] = [X_h[k - 1] - x[k - N]] e^{2\pi h j / N} + x[k] e^{-2\pi h j [N-1] / N} \quad (3.9)$$

Due to the relation

$$e^{2\pi h j / N} = e^{-2\pi h j [N-1] / N} \quad (3.10)$$

equation (3.9) can be rewritten as

$$X_h[k] = [X_h[k - 1] + x[k] - x[k - N]] e^{2\pi h j / N} \quad (3.11)$$

### 3.4 Multiple linear regression

A task that often occurs when developing models is to estimate the model parameters. The model made for the HSM will be a model based on physical fundamentals and the parameters will therefore be physical [11]. One way of determining the model parameters are by using multiple linear regression. The general multiple regression model has the form

$$Y = \beta_0 + \beta_1 X_1 + \cdots + \beta_p X_p \quad (3.12)$$

where  $Y$  is the model response,  $X = [1, X_1, \cdots, X_p]$  are the regressors of the model and  $\beta = [\beta_0, \cdots, \beta_p]$  are unknown parameters [17]. If the values of  $X$  are specified, equation (3.12) can be written as

$$y = \beta_0 + \beta_1 x_1 + \cdots + \beta_p x_p \quad (3.13)$$

Suppose data is observed for  $n$  cases. This means that  $Y$ ,  $X$  and  $\beta$  can be defined as

$$Y = \begin{pmatrix} y_1 \\ y_2 \\ \vdots \\ y_n \end{pmatrix} \quad X = \begin{pmatrix} 1 & x_{11} & \cdots & x_{1p} \\ 1 & x_{21} & \cdots & x_{2p} \\ \vdots & \vdots & \vdots & \vdots \\ 1 & x_{n1} & \cdots & x_{np} \end{pmatrix} \quad \beta = \begin{pmatrix} \beta_0 \\ \beta_1 \\ \vdots \\ \beta_p \end{pmatrix}. \quad (3.14)$$

In matrix terms (3.14) the mean function of the model response is

$$Y = X\beta. \quad (3.15)$$

An estimation of the parameters  $\beta$  can be done by using ordinary least squares (OLS) estimation. The least squares estimate  $\hat{\beta}$  of  $\beta$  is chosen to minimize the Residual Sum of Squares (RSS) function [17]. If  $y_i$  is the true output from the system and  $x_i^T$ ,  $i = 1 \cdots n$ , is the  $i$ th row of  $X$  the RSS function is

$$RSS(\beta) = \sum (y_i - x_i^T \beta)^2 = (Y - X\beta)^T (Y - X\beta). \quad (3.16)$$

The OLS estimates can be found from (3.16) by differentiation with respect to  $\beta$  in a matrix [17]. Provided that the inverse  $(X^T X)^{-1}$  exists, the OLS estimate is given by equation (3.17).

$$\hat{\beta} = (X^T X)^{-1} X^T Y \quad (3.17)$$

### 3.5 Residual analysis

To determine if a model is able to explain a data set residual analysis can be used. In this thesis the residuals will be defined as the prediction error, see equation (3.18) [11].

$$\varepsilon(t, \beta) = y(t) - \hat{y}(t; \beta) \quad (3.18)$$

A good model or estimation method should yield residuals with the properties such as the residuals are uncorrelated and have zero mean. If the residuals are

correlated, it means that there are information left in the residuals that can be used in the model or in the estimation method. If the residuals does not have zero mean, it means that the result is biased. If an estimation method gives residuals that are correlated and have zero mean this means that the estimation method can be improved. The autocorrelation (ACF) of the residuals can be used to determine if the residuals are uncorrelated [8]. The autocorrelation of a signal for time-lags  $\tau$  is

$$R(\tau) = \frac{E[(X_t - \mu)(X_{t+\tau} - \mu)]}{\sigma^2} \quad (3.19)$$

where  $\mu$  is the mean and  $\sigma^2$  is the variance [12]. If the ACF is zero for all  $\tau \neq 0$  the signal is not correlated.

To determine if the residual has zero mean it is possible to look at the histograms of the residual. A histogram is a graphical representation of the distribution of the data.

## 3.6 Extended Kalman Filter

The discrete-time Extended Kalman Filter (EKF) is a nonlinear filter that can be used to estimate the states in a time discrete nonlinear system

$$\begin{aligned} x_{k+1} &= f(x_k, u_k, v_k) & Cov(v_k) &= Q_k \\ y_k &= h(x_k, u_k, e_k) & Cov(e_k) &= R_k \\ E(x_0) &= \hat{x}_{1|0} \\ Cov(x_0) &= P_{1|0}. \end{aligned}$$

where  $v_k$  and  $e_k$  are white noise [9]. The first order EKF is applied on the state space model by using Algorithm 1. In Algorithm 1 the initial states  $\hat{x}_{1|0}$  and  $P_{1|0}$  and the covariance matrixes  $Q_k$  and  $R_k$  are seen as tuning parameters.

---

### Algorithm 1 EKF algorithm

---

$$\begin{aligned} S_k &= R + h'(\hat{x}_{k|k-1})P_{k|k-1}(h'(\hat{x}_{k|k-1}))^T \\ K_k &= P_{k|k-1}(h'(\hat{x}_{k|k-1}))^T S_k^{-1} \\ \varepsilon_k &= y_k - h(\hat{x}_{k|k-1}) \\ \hat{x}_{k|k} &= \hat{x}_{k|k-1} + K_k \varepsilon_k \\ P_{k|k} &= P_{k|k-1} - P_{k|k-1}(h'(\hat{x}_{k|k-1}))^T S_k^{-1} h'(\hat{x}_{k|k-1})P_{k|k-1} \\ \hat{x}_{k+1|k} &= f(\hat{x}_{k|k}, u_{k|k}) \\ P_{k+1|k} &= f_w(\hat{x}_{k|k}, u_{k|k})Q(f_w(\hat{x}_{k|k}, u_{k|k}))^T + f'(\hat{x}_{k|k}, u_{k|k})P_{k|k}(f'(\hat{x}_{k|k}, u_{k|k}))^T \end{aligned}$$


---

The terms  $f'(\hat{x}_{k|k}, u_{k|k})$  and  $f_w(\hat{x}_{k|k}, u_{k|k})$  are the Jacobians of the model with respect to the states and noise respectively, and  $h'(\hat{x}_{k|k-1})$  is the Jacobian of  $h(x_k, u_k, e_k)$  with respect to the states, see equation (3.22), (3.23) and (3.24).

$$f'(\hat{x}_{k|k}, u_{k|k}) = \left. \frac{\partial f}{\partial x} \right|_{x=\hat{x}_{k|k}} \quad (3.22)$$

$$f_w(\hat{x}_{k|k}, u_{k|k}) = \left. \frac{\partial f}{\partial v} \right|_{x=\hat{x}_{k|k}} \quad (3.23)$$

$$h'(\hat{x}_{k|k-1}) = \left. \frac{\partial h}{\partial x} \right|_{x=\hat{x}_{k|k-1}} \quad (3.24)$$

# 4

---

## Data collection

This chapter will first describe the equipment used to collect the data. I will continue by describing the used motor and some of its characteristics. In the end of the chapter the collected datasets and what they are used for are described.

### 4.1 Equipment setup

The hardware used for data collection is presented in Table 4.1, and the setup for data collection is shown in Figure 4.1. The motor used is a Hybrid Stepper Motor, HSM, see detailed description in Chapter 3. The given parameters for the motor are listed in Table 4.2.

To run the motor a driver, together with a demo board from Allegro is used, see Figure 4.2. The demo board has switches which makes it possible for the user to easy change settings [13]. To make the motor drive as smooth as possible mixed decay mode is used together with microstepping with 1/16 step. Mixed decay mode is a technique to obtain greater control of the phase current when it is decreasing [13]. On the driver it is also possible to set HOLD on and off. When HOLD is on, the motor generates as much torque as possible with the given power. The motor will take one step each time the step pin, see the pin-diagram in [13], goes high. To be able to create a motion a pulse train will be applied to the step pin. To perform this pulse train a waveform generator is used, with which it is possible to set a desired frequency. For collecting data it is of interest to know the motor load. With a test bench, which is used to break the motor, it is possible to set the load torque between 0 and 6 Nm.

The motor has a step angle of  $1.8^\circ$ . According to equation (3.1) this implies that the number of rotor teeth,  $p$ , are 50. When driving in full step the motor will perform  $\frac{360}{1.8} = 200$  steps per revolution. Since the motor is microstepped with 1/16 step the motor will perform  $200 \cdot 16 = 3200$  steps per revolution. This

Equipment	Function
Hybrid Stepper motor from STEGIA	The motor used for datacollection.
Agilent 33522A Waveform Generator	Used to create step pulses in desired frequency.
Agilent 0-30 V, 3A DC Power supply	Used to power up the Demo board.
Keysight MSO-X 3034T oscilloscope	Used to collect datasets.
Current probes	Used to measure phase current.
Voltage probes	Used to measure phase probes.
Allegro A3985/A3986/A4989 Demo board rev2	Used to drive the motor.
A4989 Dual Full-Bridge MOSFET Driver with Microstepping Translator	Used to drive the motor.
Hybrid Stepper Motor	The HSM from which data is collected.
Test bench for breaking the motors	Used to apply known load at the motor.

**Table 4.1:** Equipment used for data collection.

Parameter	Value
Number of phases	2
Step Angle	1.8 °
Rated Voltage	3.5 V DC
Rated Current	2.8 Amp
Holding Torque	3.0 N.m Min (Two phase on/rated current)
Phase Resistance	1.25 ohm±10% (20°C)
Phase Inductance	4.2 mH±20% (1kHz 1V rms)
Rotor Inertia	365g.cm <sup>2</sup>
Motor Weight	0.84 kg
Insulation Class	B(130°C)

**Table 4.2:** Motor parameters

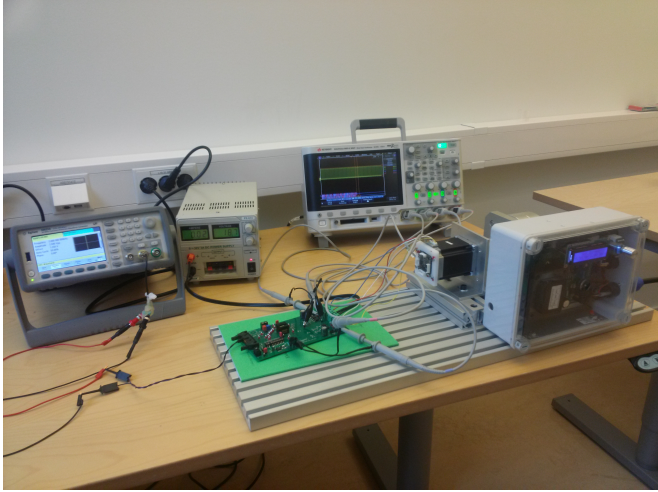


**Figure 4.1:** Setup for data collection. In the back row from left to right are the waveform generator, the power supply and the oscilloscope. In the front is the test bench for breaking together with the HSM and the Allegro Demo board.

means that 3200 pulses on the step input on the Allegro driver is needed per revolution.

The velocity of the motor is determined by the frequency on the pulse train set to the step pin on the driver. If there is no step loss on the motor the velocity of the motor will be proportional to the frequency of the pulse train. Theoretically if the step frequency is  $f$  Hz the the motor will take  $n = f$  steps/s. If the motor needs to take  $k$  steps per revolution the angular velocity can be calculated as  $\omega = \frac{2\pi n}{k}$  rad/s. Table 4.3 lists different step frequencies and corresponding motor angular velocities in rad/s.

To confirm the calculated relation between the step frequency and the angular velocity of the motor a test is performed. The motor is driven with different step frequencies and the time it takes for the motor to perform 10 revolutions is measured with a stop watch. This is performed three times per step frequency and based on the results the angular velocity is calculated as  $\frac{30}{time1+time2+time3} \cdot 2\pi$  rad/s. See the results in Table 4.4.

The squared error,  $(y - \hat{y})^2$ , of the angular velocities are listed in Table 4.5. As seen in the tables the errors are small and therefore the theoretical values for the velocity (Table 4.3) will be used in further calculations.

## 4.2 Collected Data

For modelling the motor, finding motor parameters, and test estimators, data from the motor is needed. As mentioned in Chapter 4.1 the motor is microstepped

Step frequency [kHz]	Angular velocity [rad/s]
1	1.963
1.5	2.945
2	3.927
2.5	4.909
3	5.890
3.5	6.872
4	7.854
4.5	8.836
5	9.817

**Table 4.3:** Ratio between step frequency and motor angular velocity.

Step frequency [kHz]	Average time for 10 revolutions [s]	Angular velocity [rad/s]
1	32.13	1.956
1.5	21.38	2.939
2	15.94	3.942
2.5	12.94	4.854
3	10.69	5.878
3.5	9.13	6.879
4	8.01	7.841
4.5	7.10	8.854
5	6.37	9.869

**Table 4.4:** Test to confirm the calculated velocities.

Step frequency [kHz]	$(y - \hat{y})^2$ [rad/s]
1	$0.05993 \times 10^{-3}$
1.5	$0.004133 \times 10^{-3}$
2	$0.2185 \times 10^{-3}$
2.5	$2.955 \times 10^{-3}$
3	$0.1653 \times 10^{-3}$
3.5	$0.05135 \times 10^{-3}$
4	$0.1708 \times 10^{-3}$
4.5	$0.3234 \times 10^{-3}$
5	$2.642 \times 10^{-3}$

**Table 4.5:** Squared errors between the theoretical angular velocities and the measured angular velocities.



**Figure 4.2:** Allegro demo board used to drive the motor with desired settings.

with 1/16 step. To microstep the motor makes the current sinusoidal, and the motor will obtain smooth motion. To make the current sinusoidal the voltage is pulse-width modulated and the voltage level will change very fast, up to 30 kHz, see Figure 4.3. When modelling and when determining model parameters it is advantageously to have as accurate data as possible and the rapidly changing phase voltage make high demands on the sample time of the equipment. In Figure 4.3 it is also possible to see that the current is influenced by small variations. Some of these variations are due to the pulse-width modulation and some of them are due to measurement noise. This also make demands on the equipment since it is important that the measurement noise does not hide system properties.

Different equipment for data collection, such as a BitScope model BS05, a PicoScope2203 and a Keysight MSO-X 3034T oscilloscope, were tested. For the BitScope and the PicoScope the data were covered in noise and it was hard to distinguish the signal from the noise. However the Keysight MSO-X 3034T oscilloscope showed good results when collecting data for short periods. The datasets collected are therefore only 1-2 seconds long. The datasets used in further experiment are described in Table 4.6.

Dataset	Description
7	Used in Chapter 5 to determine which parameter sets that gives highest model fit. Also used to estimate the parameters by using the EKF. The data is collected when the motor is driven at constant speed, 3.927 rad/s. There is no applied load torque.
15	Data used in Chapter 8.2 to evaluate the performance of the EKF. The data makes a step in velocity from 3.927 rad/s to 7.85 rad/s.
26	Used to evaluate the performance of the model and the EKF. The data is collected when the motor is driven at constant speed, 3.927 rad/s. There is no applied load torque.
33	Data collected when the motor stalls. Used to investigate the load angle in Chapter 7. The data is collected when the motor is driven at constant speed, 5.89 rad/s. During the data is collected to motor is stalled.
40	Data collected with the breaking bench. The applied load torque is 0 Nm and the angular velocity is 3.927 rad/s. Used to investigate the load angle in Chapter 7.
41	Data collected with the breaking bench. The applied load torque is 0.5 Nm and the angular velocity is 3.927 rad/s. Used to investigate the load angle in Chapter 7.
42	Data collected with the breaking bench. The applied load torque is 1 Nm and the angular velocity is 3.927 rad/s. Used to investigate the load angle in Chapter 7.
43	Data collected with the breaking bench. The applied load torque is 1.5 Nm and the angular velocity is 3.927 rad/s. Used to investigate the load angle in Chapter 7.
44	Data collected with the breaking bench. The applied load torque is 2 Nm and the angular velocity is 3.927 rad/s. Used to investigate the load angle in Chapter 7.
46	Data collected with the breaking bench. The applied load torque is 2.5 Nm and the angular velocity is 3.927 rad/s. Used to investigate the load angle in Chapter 7.
81	Used in Chapter 5 to determine the maximum flux linkage. The data is collected when the motor is driven at constant speed, 3.927 rad/s. There is no applied load torque.
91	Used in Chapter 5 to determine the friction constant, and used in the same chapter in the multiple linear regression. The data is collected when the motor is driven at constant speed, 3.927 rad/s and then the power is cut and the motor decelerates. There is no applied load torque.

**Table 4.6:** Data sets collected.

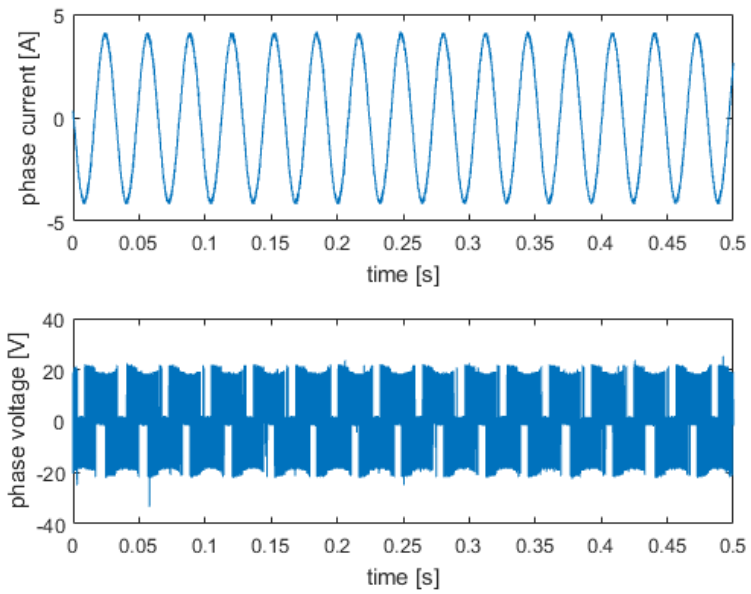


**Figure 4.3:** The appearance of the phase voltage and phase current for one phase when the motor is microstepped with 1/16 step.



# 5

---

## Modeling

This chapter will present a model of an HSM based on fundamental electrical and mechanical equations. The model will be implemented in Simulink and used in further investigations.

### 5.1 Motor model

The motor model used in the thesis is divided in an electrical and a mechanical part. An overview of the model and its parameters can be seen in figure 5.1. The back EMF induced in coil  $a$  is given by

$$e_a = \omega p \psi_m \sin(p\theta) \quad (5.1)$$

where

$\omega$  - the rotor angular velocity, [rad/s]

$p$  - the rotor teeth number

$\psi_m$  - the maximum flux linkage, [Vs/rad]

$\theta$  - the angular position of the rotor, [rad]

Similarly, the back EMF induced in coil  $b$  is given by

$$e_b = \omega p \psi_m \sin(p\theta - \lambda) \quad (5.2)$$

where  $\lambda$  is the phase angle [15]. For a motor with two stator phases  $\lambda = \frac{\pi}{2}$  and equation (5.3) can therefore be rewritten as

$$e_b = -\omega p \psi_m \cos(p\theta) \quad (5.3)$$

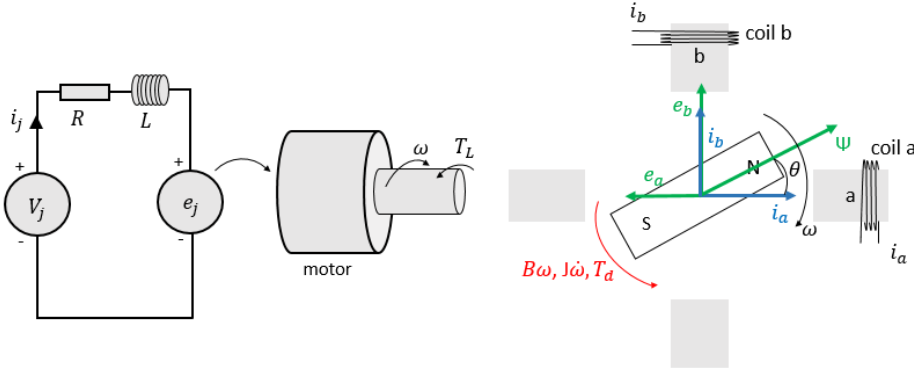


**Figure 5.1:** Illustration of the motor and motor parameters. To the left is the electrical circuit which can be related to the electrical model equations.  $V_a$  is the phase a voltage,  $i_a$  is the phase a current,  $R$  the phase resistance,  $L$  the phase inductance and  $e_a$  the back EMF for phase a. To the right is an illustration of the stator and rotor.  $\psi$  is the flux linkage,  $B$  the friction constant,  $J$  the rotor inertia,  $T_L$  the load torque,  $\theta$  is the rotor angle and  $\omega$  the rotor velocity.

The phase currents for the two phases are

$$L \frac{di_a(t)}{dt} = V_a(t) - Ri_a(t) + \omega(t)p\psi_m \sin(p\theta) \quad (5.4)$$

$$L \frac{di_b(t)}{dt} = V_b(t) - Ri_b(t) - \omega(t)p\psi_m \cos(p\theta) \quad (5.5)$$

where

$V_a, V_b$  - the phase voltages, [V]

$i_a, i_b$  - the phase currents, [A]

$R$  - the resistance of the phase windings, [Ohm]

$L$  - the phase inductance, [H]

Further the electromagnetic torque generated by the two phases are

$$T_a = i_a p \psi_m \sin(p\theta) \quad (5.6)$$

$$T_b = i_b p \psi_m \cos(p\theta) \quad (5.7)$$

Since the stator and rotor have teeth the total torque is also complemented with a component for the detent torque

$$T_d = T_{dm} \sin(2p\theta) \quad (5.8)$$

where  $T_{dm}$  is the maximum detent torque [15]. The electromagnetic torque of the motor is the sum of the phase torques and the detent torque

$$T_e = -T_a - T_b - T_d = -i_a p \psi_m \sin(p\theta) - i_b p \psi_m \cos(p\theta) - T_{dm} \sin(2p\theta) \quad (5.9)$$

The rotor motion can now be described as

$$J \frac{d\omega(t)}{dt} = T_e(t) - T_L - B\omega(t) \quad (5.10)$$

where

$J$  - the rotor inertia [ $\text{kg m}^2$ ]

$T_L$  - the load torque [ $\text{Nm}$ ]

$B$  - Friction constant [ $\text{Nms/rad}$ ]

By substituting the equation (5.9) into equation (5.10) the total equation describing the motion is obtained.

$$J \frac{d\omega(t)}{dt} = -i_a p \psi_m \sin(p\theta) - i_b p \psi_m \cos(p\theta) - T_{dm} \sin(2p\theta) - T_L - B\omega(t) \quad (5.11a)$$

$$\frac{d\theta}{dt} = \omega \quad (5.11b)$$



# 6

---

## Determination of unknown motor parameters

The unknown parameters needed for the model are the detent torque  $T_{dm}$ , the friction constant  $B$  and the maximum flux linkage  $\psi_m$ . In this section three different ways to determine the motor parameters will be presented.

### 6.1 Determination of parameters individually

This section will explain how the parameters can be determined one by one. The detent torque  $T_{dm}$  is determined by using a torque wrench and the friction constant  $B$  and the maximum flux linkage  $\psi_m$  is determined by using linear regression.

#### 6.1.1 Detent torque

The detent torque,  $T_{dm}$  can be determined by help of a torque wrench when the motor phases are unexcited. By using this method the detent torque was determined to  $T_{dm} = 0.1 Nm$ .

#### 6.1.2 Friction constant

To determine  $B$  the equation (5.11a) can be used. The motor is driven at a constant speed with no load and after a while the power is cut and data are collected during the time the motor decelerates. From the time the power is cut the phase currents,  $i_a$  and  $i_b$ , are zero and the remaining parts of equation (5.11a) is therefore

$$J \frac{d\omega(t)}{dt} = -T_{dm} \sin(2p\theta) - B\omega(t) \quad (6.1)$$

The velocity of the motor can not be measured, but because of the linear relation between the step frequency and the angular velocity it is possible to know the angular velocity of the motor before the power was cut. However it is not known how the velocity will decrease to zero and therefore an assumption is made that the velocity will decrease linearly. The dataset used to determine the parameter is dataset 91 see Chapter 4.2. Dataset 91 can also be seen in Figure 6.1 the data collected for the parameter determination is plotted. In the figure it can be seen that the power is cut at time  $t = 0.1043$ . The voltage produced after the power is cut is assumed to be the induced voltage from the motor. When the induced voltage is zero the motor has stopped.

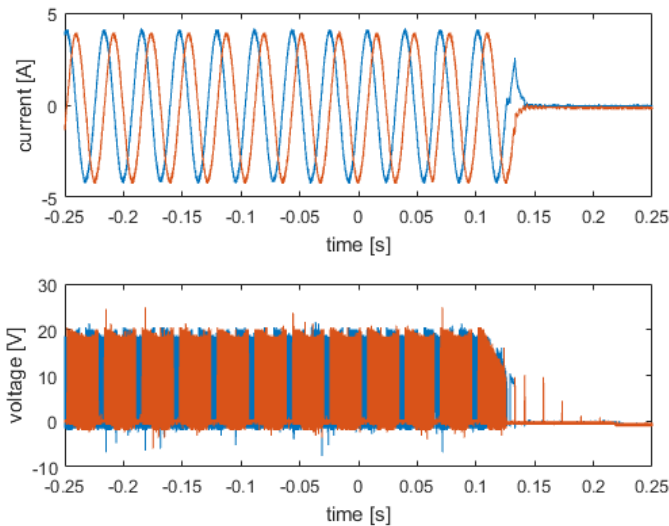


**Figure 6.1:** A picture of the data collected for determining  $B$ . The upper plot shows the phase current and the lower the phase voltage. In the lower plot a data point is added to show where the motor velocity starts to decrease. The spikes in the voltage plot at times around 0.15 is assumed to be the induced voltage in the coils. When the induced voltage is zero the motor has stopped.

With the assumption that the velocity decreases linearly, and knowledge about the time it takes for the motor to stop, it is possible to calculate  $\omega(t)$ . With knowledge of  $\omega(t)$  it is also possible to calculate the rotor acceleration and the rotor angle, see the results in Figure 6.2. In the figure, the angle  $\theta$  is plotted to start from zero radians. This means that the plotted angle is the angle the rotor rotates from the measurements begins. It is not certain that the actual rotor angle  $\theta$  starts at zero radians. Since the motor is microstepped with  $1/16$  step the motor will perform  $0.1125^\circ = 0.000625\pi \text{ rad}$  each step. This means that the rotor angle, when the measurement starts, can be  $n \times 0.000625\pi \text{ rad}$ , where  $n = 0, 1, \dots, 3200$ .

When determining the friction constant, knowledge of the angle  $2p\theta = 100\theta$  in equation (6.1) is of interest. The start angle can be  $100\theta = n \times 0.0625\pi$ .

To cover all possible angles it is only necessary to test angles between 0 and  $2\pi$  which means that  $n$  can be reduced to  $n = 0, 1, \dots, 32$ .

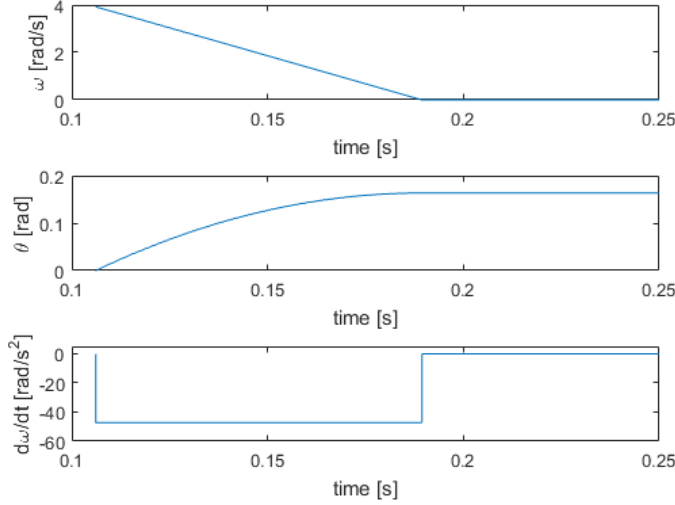


**Figure 6.2:** Assumed appearance of angular velocity and corresponding angle and acceleration.

With knowledge of the signals presented in Figure 6.2 and information about the angular offset,  $B$  can be determined with linear regression.

$$-B = \text{inv}(X^T X) X^T Y \quad (6.2)$$

where

$$Y = J \frac{d\omega(t)}{dt} + T_{dm} \sin(2p\theta)$$

$$X = \omega(t)$$

In Figure 6.3 values for  $B$  are plotted for all offsets. According to the calculations  $B$  is between  $-0.003764$  Nms/rad and  $0.005078$  Nms/rad.

The assumption that the velocity decreases linearly to zero may not be correct. A more accurate assumption may be given by examine equation (6.1). The equation is an Ordinary Differential Equation (ODE) and the solution of an ODE is an exponential function. Therefore a more correct assumption may be that the velocity decreases exponential to zero. If assuming that the detent torque is small equation (6.1) can be rewritten as

$$J \frac{d\omega}{dt} = -B\omega \Leftrightarrow$$

$$J \frac{1}{B\omega} d\omega = -dt.$$

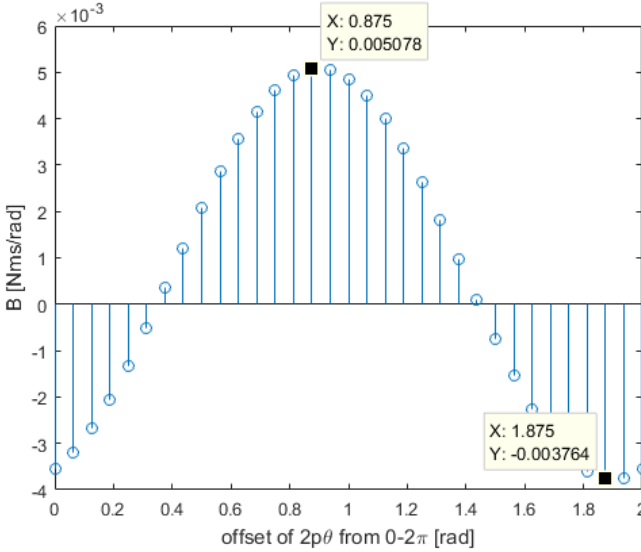


**Figure 6.3:** Calculated values for  $B$  when  $2p\theta$  has an offset between  $0$  and  $2\pi$  rad.

To solve the differential equation, integrate both sides

$$\int J \frac{1}{B\omega} d\omega = \int -dt \Rightarrow$$

$$\frac{J}{B} \log |\omega| = -t + C_1 \Rightarrow$$

$$\omega = \pm \exp\left(\frac{B}{J}(-t + C_1)\right) = \pm C \exp\left(-\frac{B}{J}t\right)$$

Before the power is cut the velocity  $\omega$  is known. This means that the parameter  $C$  can be determined as  $C = \omega(0)$ . The solution to the ode will therefore be

$$\omega = \omega(0) \exp\left(-\frac{B}{J}t\right) \quad (6.3)$$

The drawback is that both the angular velocity  $\omega$  and  $B$  is unknown and therefore it is not possible to use linear regression to determine  $B$ .

### 6.1.3 Maximum flux linkage

To determine the maximum flux linkage,  $\psi_m$ , equation (5.4) or (5.5) can be used. The equation (5.4) can be rewritten as

$$L \frac{di_a(t)}{dt} - V_a(t) + Ri_a(t) = w(t)p\psi_m \sin(p\theta)$$

The data needed can be obtained by letting the motor drive with constant velocity  $\omega$  and measure the phase voltage and phase current of one phase, see dataset 81 in Chapter 4.2. Since all parameters in equation (5.4) except the maximum flux linkage is known, or can be measured, the maximum flux linkage can be determined by linear regression where

$$Y = L \frac{di_a(t)}{dt} - V_a(t) + Ri_a(t)$$

$$X = w(t)p \sin(p\theta).$$

As previous the offset of theta is unknown and it is of interest to know the start value of the angle  $p\theta$  in equation (5.4). The offset is  $n \times 0.000625\pi \text{ rad}$ ,  $n = 0, 1, \dots, 3200$ . The angle from equation (5.4) can take the start value  $p\theta = 50\theta = n \times 0.0313$ . It is only necessary to test values between 0 and  $2\pi$  and therefore  $n$  can be reduced to  $n = 0, 1, \dots, 64$ . The maximum flux linkage,  $\psi_m$ , is therefore calculated for angles of  $n \times 0.0313$  where  $n = 0, 1, \dots, 64$ . As seen in Figure 6.4,  $\psi_m$  is between 0.02394 Vs/rad and -0.02394 Vs/rad.

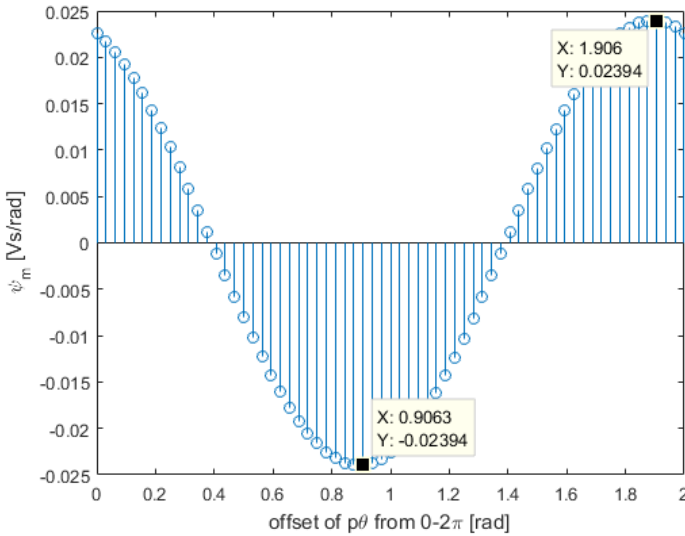


**Figure 6.4:** Calculated values for  $\psi_m$  when  $p\theta$  has an offset between 0 and  $2\pi$  rad.

To find the best value of the parameters  $B$  and  $\psi_m$ , different combinations are tested in the model, and the model is run with dataset 7, see Chapter 4.2, where the motor is driven at constant speed, 3.927 rad/s. The error  $y - \hat{y}$  is then calculated for the angle  $\theta$  and angular velocity  $\omega$ . The parameters that gave the smallest prediction error were  $B = 0.0042 \text{ Nms/rad}$  and  $\psi_m = 0.0036 \text{ Vs/rad}$  and the corresponding prediction error can be seen in Figure 6.5. A model simulation with the corresponding parameters and when dataset 7, see Chapter 4.2, is used

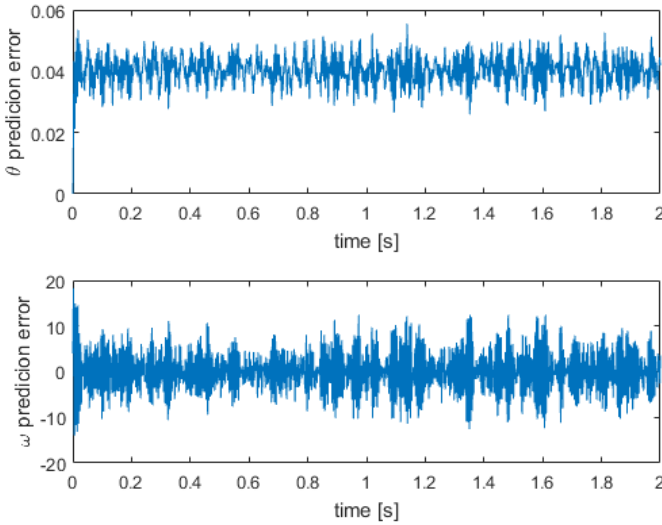


**Figure 6.5:** Prediction error when the parameters  $T_{dm} = 0.1 Nm$ ,  $B = 0.0042$  Nms/rad and  $\psi_m = 0.0036$  Vs/rad are used.

as input can be seen in Figure 6.6. As seen in Figure 6.6 the angular velocity  $\omega$  varies much. The reason can be that the motor takes steps and therefore the angle will oscillate a bit for each step, which in turn affects the angular velocity.

To investigate if the model describes the data in a good way the residuals  $\varepsilon(t, \beta) = y(t) - \hat{y}(t; \beta)$  are calculated and studied. As mentioned in Chapter 3 the model describes the data well if the residuals are uncorrelated and has mean zero. The ACF of the residuals can be seen in Figure 6.7 and the histograms can be seen in Figure 6.8. In the plot for the ACF it can be seen that correlation is not zero for all lags  $\tau \neq 0$ . This indicates that the residuals contain information that can be included in the model. In the histograms is possible to see that the residual for the angle  $\theta$  has a small bias,  $< 0.04$ .

## 6.2 Determination with multiple linear regression

Another way to estimate the parameters is to again use equation (5.11a) together with multiple linear regression as

$$Y = AX$$

where

$$Y = J \frac{d\omega(t)}{dt}$$

$$A = \begin{bmatrix} a_1 & a_2 & a_3 \end{bmatrix} = \begin{bmatrix} \psi_m & T_{dm} & B \end{bmatrix}$$

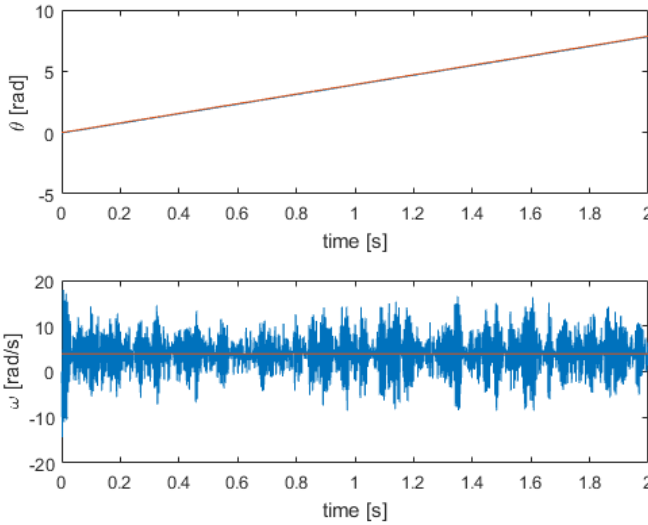


**Figure 6.6:** The states from the simulink model when  $T_{dm} = 0.1 \text{ Nm}$   $B = 0.0042 \text{ Nms/rad}$  and  $\psi_m = 0.0036 \text{ Vs/rad}$ . The red curve in the upper left plot and lower left plot are the theoretical values of  $\theta$  and  $\omega$ , the blue comes from the model with the above mentioned parameters.

$$X = \begin{bmatrix} x_1 \\ x_2 \\ x_3 \end{bmatrix} = \begin{bmatrix} -i_a p \sin(p\theta) - i_b p \cos(p\theta) \\ -\sin(2p\theta) \\ -w \end{bmatrix}$$

And the parameters will be determined by

$$A = \text{inv}(X^T X) X^T Y \quad (6.4)$$

The data used is dataset 91 which is the data used to calculate B earlier, but here also the measured signals  $i_a$  and  $i_b$  are used in the estimation. As previous the offset of  $\theta$  is unknown and parameters are calculated for different offsets. The result is shown in Figure 6.9.

Combinations of the parameters are tested in the simulink model and the prediction error  $y - \hat{y}$  is calculated for all parameter sets. The parameters that gave the smallest prediction error were

$$\psi_m = -8.796 \times 10^{-6} \text{ [Vs/rad]}$$

$$T_{dm} = 4.692 \times 10^{-5} \text{ [Nm]}$$

$$B = 2.535 \times 10^{-5} \text{ [Nms/rad]}$$

see the corresponding prediction error in Figure 6.10. A model simulation with the parameters and when dataset 7, see Chapter 4.2, is used as input can be seen in Figure 6.11. As seen in figure 6.11 the parameters are not able to describe the real system and the parameter set is therefore rejected.

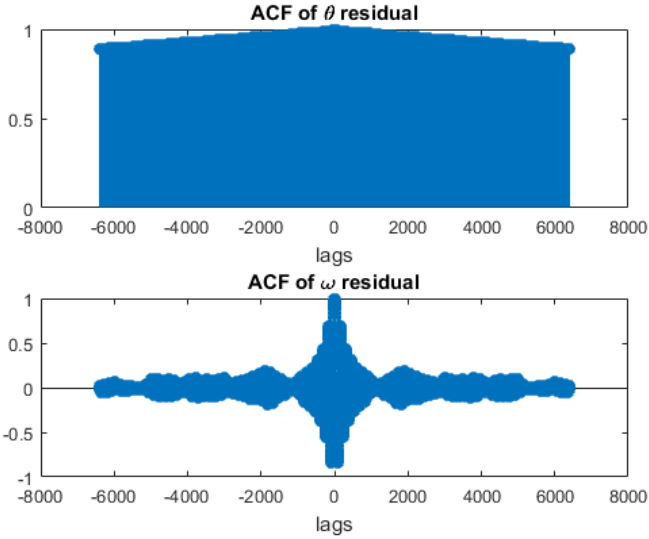


**Figure 6.7:** Autocorrelation of the residuals for the parameter set  $T_{dm} = 0.1Nm$ ,  $B = 0.0042 Nms/rad$  and  $\psi_m = 0.0036 Vs/rad$ .

### 6.3 Determination with the Extended Kalman Filter

Another method to determine the unknown parameters is to use the Extended Kalman Filter, EKF. As described in Chapter 3.6 the EKF is used to determine the states in a discrete nonlinear state space model. With the motor model equations from Chapter 5 the following state space model can be obtained.

$$\begin{aligned} \dot{x} &= a(x, u, d) \\ y &= Cx \end{aligned} \quad (6.5)$$

where

$$x = \begin{bmatrix} i_a \\ i_b \\ \omega \\ \theta \end{bmatrix} \quad u = \begin{bmatrix} V_a \\ V_b \end{bmatrix} \quad d = T_L \quad C = \begin{bmatrix} 1 & 0 & 0 & 0 \\ 0 & 1 & 0 & 0 \end{bmatrix}$$

$$a(x, u, d) = \begin{cases} \frac{1}{L}(u_1 - Rx_1 + x_3\psi_m p \sin(px_4)) \\ \frac{1}{L}(u_2 - Rx_2 - x_3\psi_m p \cos(px_4)) \\ \frac{1}{J}(-x_1\psi_m p \sin(px_4) - x_2\psi_m p \cos(px_4) - T_{dm} \sin(2px_4) - d - Bx_3) \\ x_3 \end{cases}$$

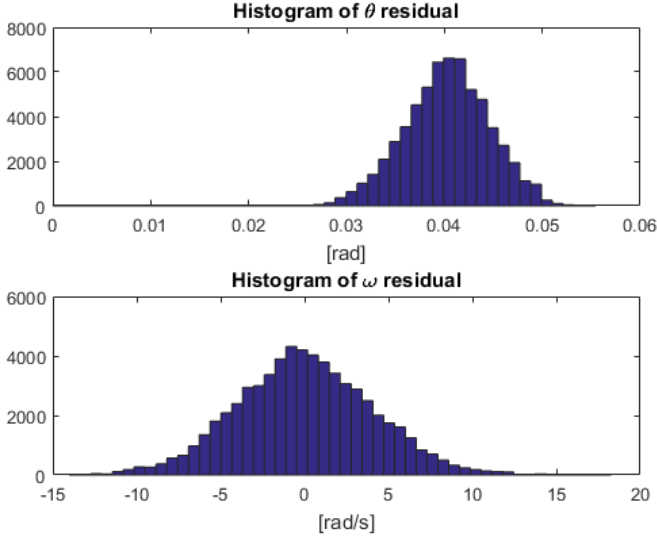


**Figure 6.8:** Histogram of the residuals for the parameter set  $T_{dm} = 0.1 Nm$ ,  $B = 0.0042 Nms/rad$  and  $\psi_m = 0.0036 Vs/rad$ .

By adding the unknown parameters as states and assuming that the parameters are constant the following can be added to the state space model (6.5)

$$\begin{aligned}
 T_{dm} &= x_5, & \dot{x}_5 &= 0 \\
 \psi_m &= x_6, & \dot{x}_6 &= 0 \\
 B &= x_7, & \dot{x}_7 &= 0
 \end{aligned} \tag{6.6}$$

The linear state space model (6.5) is extended as

$$\begin{aligned}
 \dot{x} &= a(x, u, d) \\
 y &= Cx
 \end{aligned} \tag{6.7}$$

where

$$x = \begin{bmatrix} i_a \\ i_b \\ \omega \\ \theta \\ T_{dm} \\ \psi_m \\ B \end{bmatrix} \quad u = \begin{bmatrix} V_a \\ V_b \end{bmatrix} \quad d = T_L \quad C = \begin{bmatrix} 1 & 0 & 0 & 0 & 0 & 0 & 0 \\ 0 & 1 & 0 & 0 & 0 & 0 & 0 \end{bmatrix}$$

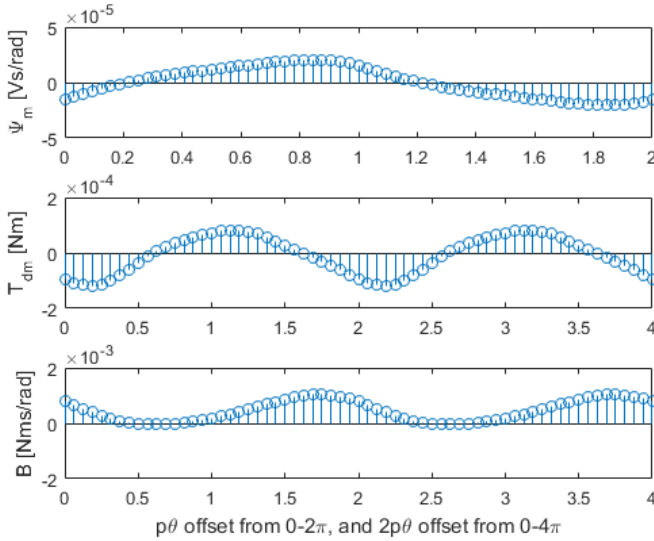


**Figure 6.9:** Estimated values for the unknown parameters.

$$a(x, u, d) = \begin{cases} \frac{1}{L}(u_1 - Rx_1 + x_3\psi_m p \sin(px_4)) \\ \frac{1}{L}(u_2 - Rx_2 - x_3\psi_m p \cos(px_4)) \\ \frac{1}{J}(-x_1\psi_m p \sin(px_4) - x_2\psi_m p \cos(px_4) - T_{dm} \sin(2px_4) - d - Bx_3) \\ x_3 \\ 0 \\ 0 \\ 0 \end{cases}$$

The state space model above is nonlinear and time continuous. To discretize the linear model Euler forward is used according to

$$x_{k+1} = x_k + T\dot{x} \quad (6.8)$$

where  $T$  is the sampling time. The discretized state space model of the motor can then be written as

$$x_{k+1} = x_k + T(a(x_k, u_k, d_k, v_k)) = f(x_k, u_k, d_k, v_k) \quad (6.9a)$$

$$y_k = Hx_k = h(x_k, e_k) \quad (6.9b)$$

where  $H = C$  and  $v_k$  and  $e_k$  are white noise. Further on the load torque  $T_L$  is seen as an unknown disturbance and will in further calculations be merged with the noise  $v_k$ . The EKF can now be applied on the discrete state space model (6.9) by using Algorithm 1.

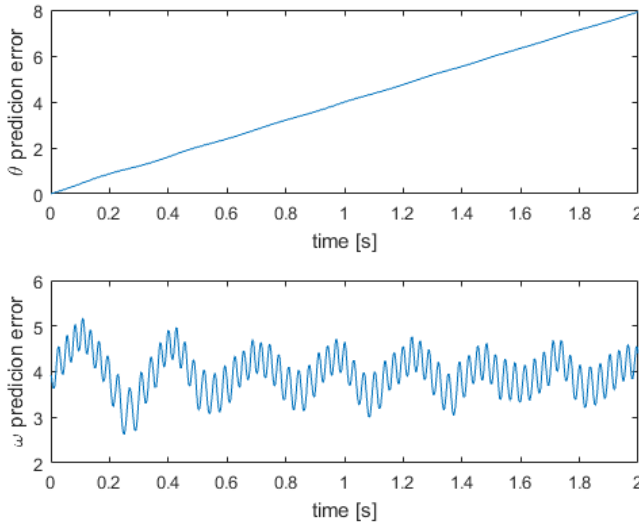


**Figure 6.10:** Prediction error for the parameter set  $T_{dm} = 4.692 \times 10^{-5} \text{ Nm}$ ,  $B = 2.535 \times 10^{-5} \text{ Nms/rad}$ ,  $\psi_m = -8.796 \times 10^{-6} \text{ Vs/rad}$ .

### 6.3.1 Choose filter parameters

Design parameters for the EKF are the initial state  $x_{0|0}$  and the covariance of the initial state  $P_{0|0}$ . Also the covariance matrixes  $Q$  and  $R$ , and the noise matrix  $f_w$  needs to be chosen. There is no exact method for selecting the parameters but, there are some guidelines discussed in [3]. The initial state will be chosen as close to the known initial value as possible, and the covariance matrix  $P_{0|0}$  represents the confidence about the initial state. The  $Q$  matrix is connected to the model noise. Increasing  $Q$  could either be seen as an indication of system noise or it can be seen as an increase of model uncertainty [3]. The  $R$  matrix is instead connected to the measurement noise. Increasing  $R$  indicates that the measurements are affected by noise and cannot be trusted as much. It is common to choose the  $P_{0|0}$ ,  $Q$  and  $R$  as diagonal matrices. According to [3] this is due to the lack of information about the off-diagonal terms and also because the fact that the off-diagonal terms often is significantly smaller than the diagonal terms. The last matrix is the noise matrix  $f_w$ . Since all noise affecting the estimates is not modeled this matrix can be seen as a tuning parameter explaining the magnitude of the noise rather than the Jacobian of the model with respect to the noise.

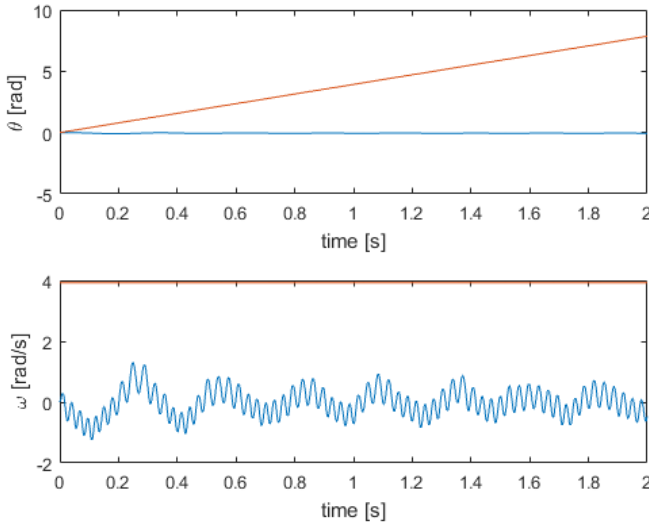


**Figure 6.11:** The estimated signals from the simulink model for the parameter set  $T_{dm} = 4.692 \times 10^{-5}$  Nm,  $B = 2.535 \times 10^{-5}$  Nms/rad,  $\psi_m = -8.796 \times 10^{-6}$  Vs/rad. The red curve in the upper left plot and lower left plot are the theoretical values of  $\theta$  and  $\omega$ . The blue comes from the model with the calculated parameters.

With the above thoughts in mind the matrices are chosen as:

$$x_{0|0} = \begin{bmatrix} 0 \\ 0 \\ \omega_{ref} \\ 0 \\ 0 \\ 0 \\ 0 \\ 0 \end{bmatrix} \quad P_{0|0} = \begin{bmatrix} 10 & 0 & 0 & 0 & 0 & 0 & 0 \\ 0 & 10 & 0 & 0 & 0 & 0 & 0 \\ 0 & 0 & 1 \cdot 10^{-2} & 0 & 0 & 0 & 0 \\ 0 & 0 & 0 & 1 \cdot 10^{-2} & 0 & 0 & 0 \\ 0 & 0 & 0 & 0 & 1 & 0 & 0 \\ 0 & 0 & 0 & 0 & 0 & 1 & 0 \\ 0 & 0 & 0 & 0 & 0 & 0 & 1 \end{bmatrix}$$

$$f_w = \begin{bmatrix} 1 & 0 & 0 & 0 & 0 & 0 & 0 \\ 0 & 1 & 0 & 0 & 0 & 0 & 0 \\ 0 & 0 & 10 & 0 & 0 & 0 & 0 \\ 0 & 0 & 0 & 0 & 0 & 0 & 0 \\ 0 & 0 & 0 & 0 & 1 \cdot 10^{-3} & 0 & 0 \\ 0 & 0 & 0 & 0 & 0 & 1 \cdot 10^{-3} & 0 \\ 0 & 0 & 0 & 0 & 0 & 0 & 1 \cdot 10^{-3} \end{bmatrix}$$

$$Q = \begin{bmatrix} 1 & 0 & 0 & 0 & 0 & 0 & 0 \\ 0 & 1 & 0 & 0 & 0 & 0 & 0 \\ 0 & 0 & 1 \cdot 10^{-1} & 0 & 0 & 0 & 0 \\ 0 & 0 & 0 & 1 \cdot 10^{-3} & 0 & 0 & 0 \\ 0 & 0 & 0 & 0 & 1 \cdot 10^{-3} & 0 & 0 \\ 0 & 0 & 0 & 0 & 0 & 1 \cdot 10^{-3} & 0 \\ 0 & 0 & 0 & 0 & 0 & 0 & 1 \cdot 10^{-3} \end{bmatrix} \quad R = \begin{bmatrix} 1 \cdot 10^{-1} & 0 \\ 0 & 1 \cdot 10^{-1} \end{bmatrix}$$

The result of the parameter estimation when using dataset 7, see Chapter 4.2, can be seen in Figure 6.12. Of interest is to look at the covariance matrix for

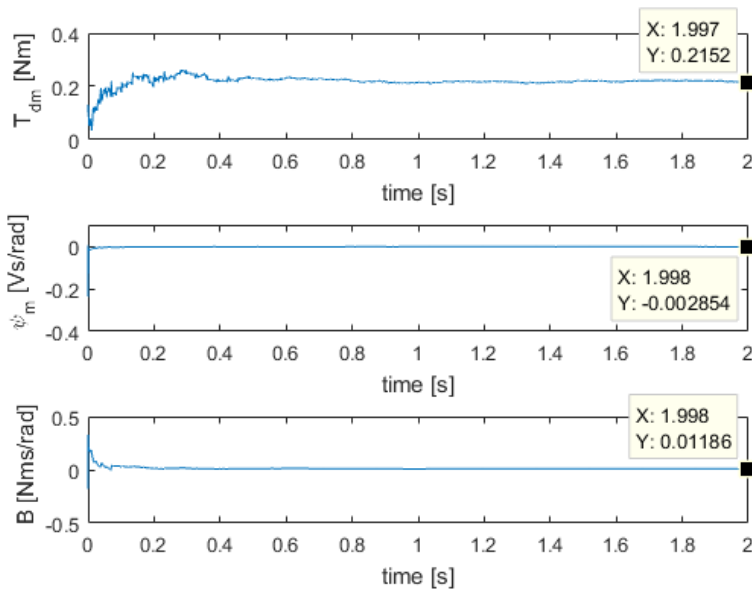


*Figure 6.12: Result of the parameter estimation using the EKF.*

the estimated states to examine if the standard deviation is in the same order as the estimated parameters. If the standard deviation is significantly larger than the parameters the estimation is uncertain. The estimated parameters and corresponding variances and standard deviations are shown in Table 6.1. As seen in Table 6.1 the estimated parameters have the same size as the corresponding standard deviation and the parameter estimation is therefore valid.

## 6.4 Residual analysis

From the parameter determination above two different parametersets were proposed. From Chapter 6.1 a parameter set was given for the unknown parameters

Parameter	Estimated value	Variance	Standard deviation
$T_{dm}$	0.2152	0.023526	0.153382
$\psi_m$	-0.002854	0.000007	0.002646
B	0.01186	0.000210	0.014491

**Table 6.1:** The variances and standard deviation for the estimated parameters.

according to:  $T_{dm} = 0.1 Nm$ ,  $B = 0.0042 Nms/rad$  and  $\psi_m = 0.0036 Vs/rad$ . Parameter estimation with the EKF in Chapter 6.3 resulted in the parameter set:  $T_{dm} = 0.2152 Nm$ ,  $B = 0.01186 Nms/rad$  and  $\psi_m = -0.002854 Vs/rad$ . To validate the parameters, residual analysis is applied. The model is tested on with a new dataset, in other words, not the dataset that were used to determine the parameters. Data 26, see Chapter 4.2, is used as input to the model and the simulation result for the angle  $\theta$  and angular velocity  $\omega$  can be seen in Figure 6.13. The histograms of the residuals  $y - \hat{y}$  can be seen in Figure 6.14. In the histograms it is possible to see if the residuals are biased or not. In Figure 6.14 it can be seen that both parameter sets causes small bias. For the  $\theta$ -,  $\omega$ - and  $i_b$ -residual the parameter set determined by the EKF gives a slightly smaller bias. For the  $i_a$ -residual the parameterset determined in Chapter 6.1 give a slightly smaller bias. The ACF of the residuals are shown in Figure 6.15. From the ACF it is possible to see if the residuals are correlated in time. If the residuals were not autocorrelated the ACF would have been equal to zero for all lags except lag zero. In Figure 6.15 it can be seen that the residuals are more or less correlated. This means that there are more information in the residuals that can be added in the model.

The model and the model parameters shall be chosen in a way that it is possible for the model to serve it's purpose. The purpose of the model is to be used in the EKF for estimating the rotor angle, and angular velocity. Since the residual from the parameterset  $T_{dm} = 0.2152 Nm$ ,  $B = 0.01186 Nms/rad$  and  $\psi_m = -0.002854 Vs/rad$  gives a smaller bias and were less correlated for the  $\theta$  and  $\omega$  residual the result of this analysis is that the parameterset  $T_{dm} = 0.2152 Nm$ ,  $B = 0.01186 Nms/rad$  and  $\psi_m = -0.002854 Vs/rad$  is able to describe the real system slightly better than the parameterset  $T_{dm} = 0.1 Nm$ ,  $B = 0.0042 Nms/rad$  and  $\psi_m = 0.0036 Vs/rad$ .

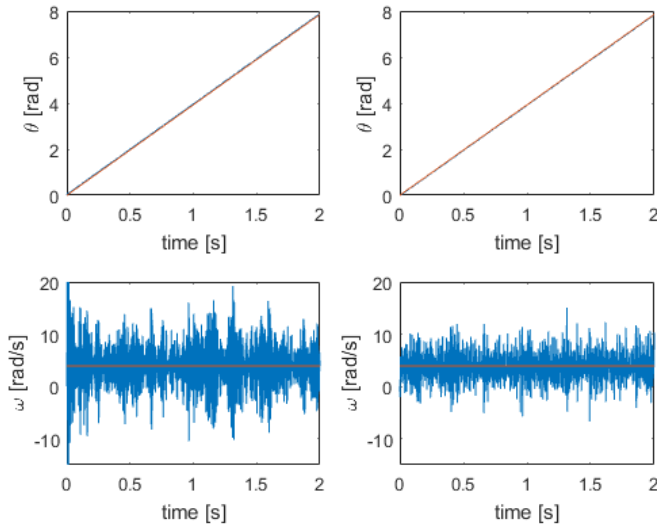


**Figure 6.13:** The figures in the left column are the result from a simulation when the parameters  $T_{dm} = 0.1Nm$ ,  $B = 0.0042Nms/rad$  and  $\psi_m = 0.0036Vs/rad$  are used. The figures in the right column are the result from a simulation when the parameters  $T_{dm} = 0.2152Nm$ ,  $B = 0.01186Nms/rad$  and  $\psi_m = -0.002854Vs/rad$  are used. The red curve represent the precalculated  $\theta$  and  $\omega$  and the blue is the results from the simulations.

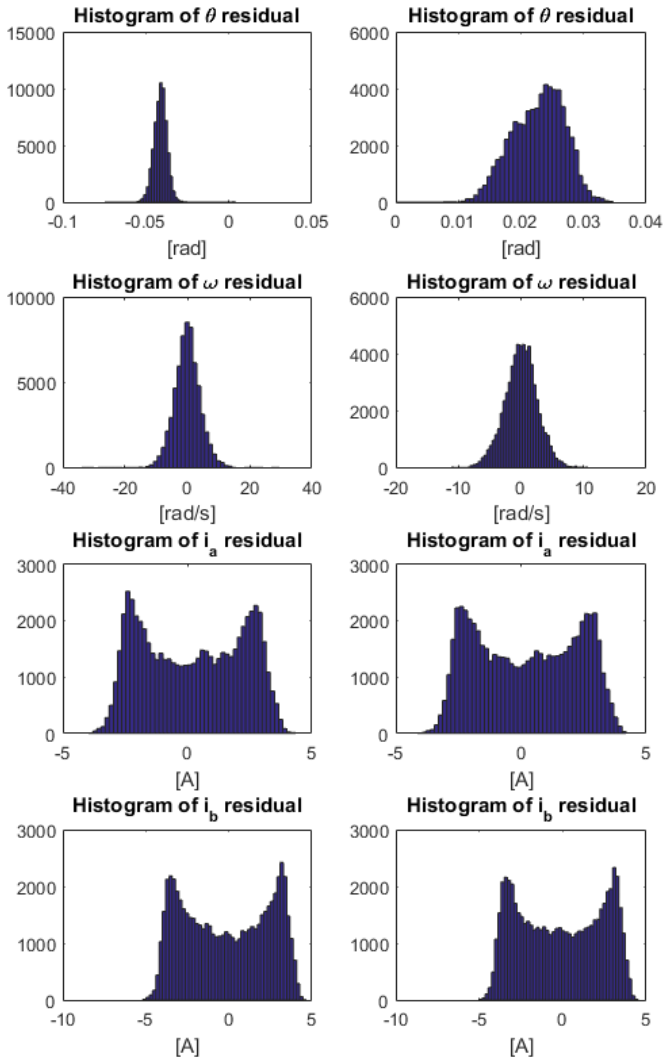


**Figure 6.14:** The figures in the left column are the histograms of the residuals for  $\theta$  and  $\omega$  for the parameters  $T_{dm} = 0.1 Nm$ ,  $B = 0.0042 Nm/s/rad$  and  $\psi_m = 0.0036 Vs/rad$ . The figures in the right column are the histograms for the residuals when the parameters  $T_{dm} = 0.2152 Nm$ ,  $B = 0.01186 Nm/s/rad$  and  $\psi_m = -0.002854 Vs/rad$  are used.

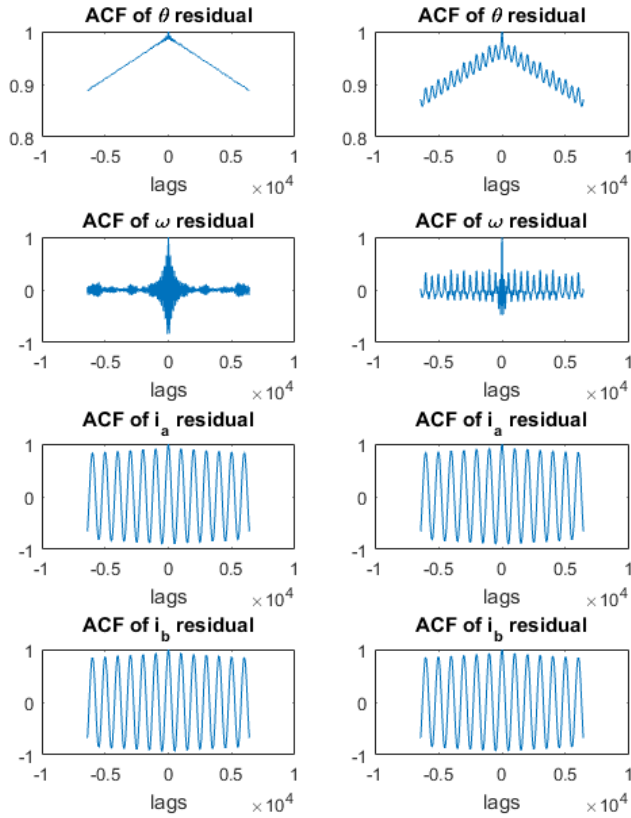


**Figure 6.15:** The figures in the left column are the ACF of the residuals for  $\theta$  and  $\omega$  for the parameters  $T_{dm} = 0.1Nm$ ,  $B = 0.0042Nms/rad$  and  $\psi_m = 0.0036Vs/rad$ . The figures in the right column are the ACF for the residuals when the parameters  $T_{dm} = 0.2152Nm$ ,  $B = 0.01186Nms/rad$  and  $\psi_m = -0.002854Vs/rad$  are used.



# 7

---

## Estimations

This chapter will describe the estimation methods used in this thesis. In the first section the Extended Kalman Filter is implemented to estimate the rotor angle and rotor position. In the next section the load angle estimation is described and implemented.

### 7.1 Extended Kalman Filter

An Extended Kalman Filter (EKF) can be used to estimate the rotor angular velocity and the angle the rotor has rotated from the estimation started. As described in Chapter 3.6 the EKF is used to determine the states in a discrete nonlinear state space model. With the motor model equations from Chapter 5 the following state space model can be obtained.

$$\begin{aligned}\dot{x} &= a(x, u, d) \\ y &= Cx\end{aligned}\tag{7.1}$$

where

$$x = \begin{bmatrix} i_a \\ i_b \\ \omega \\ \theta \end{bmatrix} \quad u = \begin{bmatrix} V_a \\ V_b \end{bmatrix} \quad d = T_L \quad C = \begin{bmatrix} 1 & 0 & 0 & 0 \\ 0 & 1 & 0 & 0 \end{bmatrix}$$

$$a(x, u, d) = \begin{cases} \frac{1}{L}(u_1 - Rx_1 + x_3\psi_m p \sin(px_4)) \\ \frac{1}{L}(u_2 - Rx_2 - x_3\psi_m p \cos(px_4)) \\ \frac{1}{J}(-x_1\psi_m p \sin(px_4) - x_2\psi_m p \cos(px_4) - T_{dm} \sin(2px_4) - d - Bx_3) \\ x_3 \end{cases}$$

The state space model above is nonlinear and time continuous. To discretize the linear model Euler forward is used according to

$$x_{k+1} = x_k + T\dot{x} \quad (7.2)$$

where T is the sampling time. The discretized state space model of the motor can then be written as

$$x_{k+1} = x_k + T(a(x_k, u_k, d_k, v_k)) = f(x_k, u_k, d_k, v_k) \quad (7.3a)$$

$$y_k = Hx_k = h(x_k, e_k) \quad (7.3b)$$

where  $H = C$  and  $v_k$  and  $e_k$  are white noise. Further on the load torque  $T_L$  is seen as an unknown disturbance and will in further calculations be merged with the noise  $v_k$ . The EKF can now be applied on the discrete state space model (7.3). The first order EKF is applied on the state space model by using Algorithm 1.

As described in Chapter 6.3.1, design parameters for the EKF are the initial state  $x_{0|0}$ , the covariance of the initial state  $P_{0|0}$  and the covariance matrixes Q and R, and the noise matrix  $f_w$ . By using the guidelines described in Chapter 6.3.1, the matrices are chosen as:

$$x_{0|0} = \begin{bmatrix} 0 \\ 0 \\ \omega_{ref} \\ 0 \end{bmatrix} \quad P_{0|0} = \begin{bmatrix} 5 & 0 & 0 & 0 \\ 0 & 5 & 0 & 0 \\ 0 & 0 & 1 \cdot 10^{-2} & 0 \\ 0 & 0 & 0 & 6 \end{bmatrix} \quad f_w = \begin{bmatrix} 1 & 0 & 0 & 0 \\ 0 & 1 & 0 & 0 \\ 0 & 0 & 10 & 0 \\ 0 & 0 & 0 & 0 \end{bmatrix}$$

$$Q = \begin{bmatrix} 1 & 0 & 0 & 0 \\ 0 & 1 & 0 & 0 \\ 0 & 0 & 1 \cdot 10^{-1} & 0 \\ 0 & 0 & 0 & 1 \cdot 10^{-3} \end{bmatrix} \quad R = \begin{bmatrix} 1 & 0 \\ 0 & 1 \end{bmatrix}$$

## 7.2 Load angle estimation

To get knowledge about the load torque [7] proposes to determine the load angle, see description in Chapter 3.2. As mentioned in Chapter 3.2 the load angle can be determined by knowledge of the phase current and the back EMF. The current vector  $i_s$  can be measured leaving only determining of the back EMF.

To estimate the back EMF equation (5.4), describing the electrical relations in the stator phase, can be used. The equation can be rewritten as:

$$e_s = u_s - L_s \frac{di_s}{dt} - R_s i_s \quad (7.4)$$

One possibility to estimate the back EMF is by solving equation (7.4), but since the current is a noisy signal it is not recommended. Instead the authors in [7] suggests to write equation (7.4) in the frequency domain.

$$E_s(j\omega_1) = U_s(j\omega_1) - j\omega_1 L_s I_s(j\omega_1) - R_s I_s(j\omega_1) \quad (7.5)$$

where  $\omega_1$  is the fundamental frequency [7]. To determine  $\omega_1$ , the fundamental voltage  $U_{s1}$  and fundamental current  $I_{s1}$  authors in [7] suggests to use the SDFT, see Chapter 3.3. With knowledge of the back EMF the load angle can be determined according to

$$\hat{\delta} = \frac{\pi}{2} - (\angle(E_{s1}) - \angle(I_{s1})) \quad (7.6)$$

The data used for calculating the load angle are dataset 33, 40, 41, 42, 43, 44 and 46, which is data collected with the breaking bench for load torques between 0-2.5 Nm, see Chapter 4.2. The datasets contains of collected phase voltages and phase currents for the two phases respectively.

To obtain the current vector  $i_s$  and the voltage vector  $u_s$  the phase currents  $i_a$  and  $i_b$  respective the phase voltages  $u_a$  and  $u_b$  are added together according to

$$i_s = i_a + ji_b \quad (7.7)$$

$$u_s = u_a + ju_b \quad (7.8)$$

This addition will preserve the information about the direction of the vectors. The SDFT is then used to calculate  $I_s$  and  $U_s$ , and then the load angle  $\hat{\delta}$ . The relation between the load torque and the load angle, when angular velocity is 3.927 rad/s and at maximum rated current 1.8 ampere, can be seen in Figure 7.1. When the rotor is stalled the load angle will increase  $\pi/2$ . In Figure 7.2 it is shown how the load angle can vary when the rotor is completely stalled.

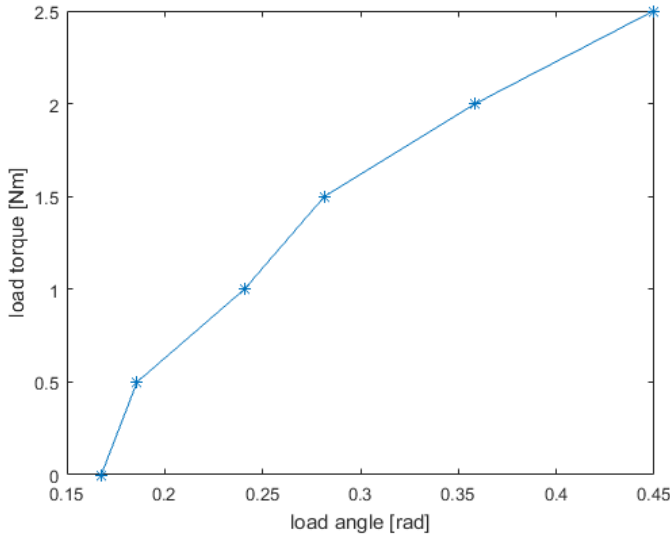


**Figure 7.1:** The relation between the load torque and load angle for  $\omega = 3.927$  rad/s.

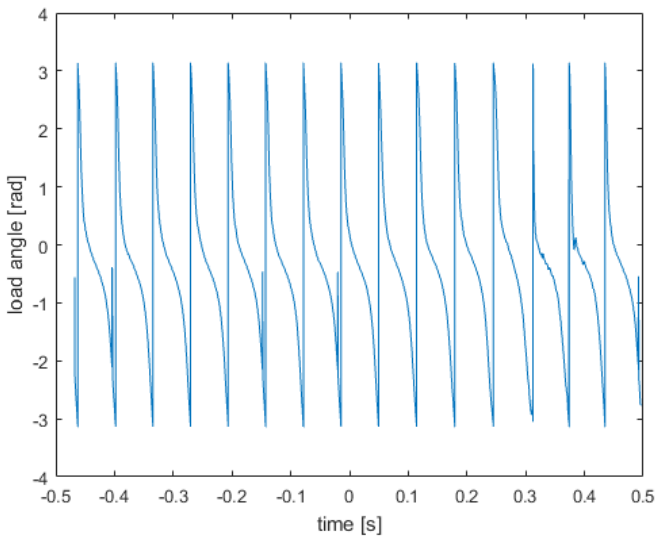


**Figure 7.2:** *The appearance of the load angle when the motor is completely stalled.*

# 8

---

## Results

In this chapter the results from this thesis work will be presented. In Section 8.1 the model together with the determined parameters will be evaluated for different datasets. The model is used in the EKF to estimate the rotor angle and angular velocity. The results from this estimations is presented in section 8.2. Finally an evaluation of the load angle estimations is presented in section 8.3.

### 8.1 Evaluation of model and model parameters

From Chapter 6 it was determined that the parameterset  $T_{dm} = 0.2152Nm$ ,  $B = 0.01186Nms/rad$  and  $\psi_m = -0.002854Vs/rad$ , which was determined by the EKF, were the best parameterset for the model. To evaluate the model it is tested on with a new dataset, in other words, not the dataset that were used to determine the parameters. The dataset used will be dataset 15, see Chapter 4.2. Dataset 15 is a dataset where the motor will take a step in velocity from 3.927 rad/s to 7.854 rad/s and is used to see how the model will perform in a more difficult environment. In Figure 8.1 it is possible to see that the model is able to follow the theoretical angle well when dataset 15 is used. The estimations of the velocity is oscillating around the theoretical value, but the mean is close to the theoretical value. In Figure 8.2 the current from the model can be seen. The frequency of the current is able to follow the measured but the amplitude is to high. Also the residuals  $y - \hat{y}$  are studied. The histograms of the residuals can be seen in Figure 8.3 and the ACF can be seen in Figure 8.4. It is possible to se that the residuals only suffers from small biases, and are more or less correlated. This means that there are more information in the residuals that can be added in the model.

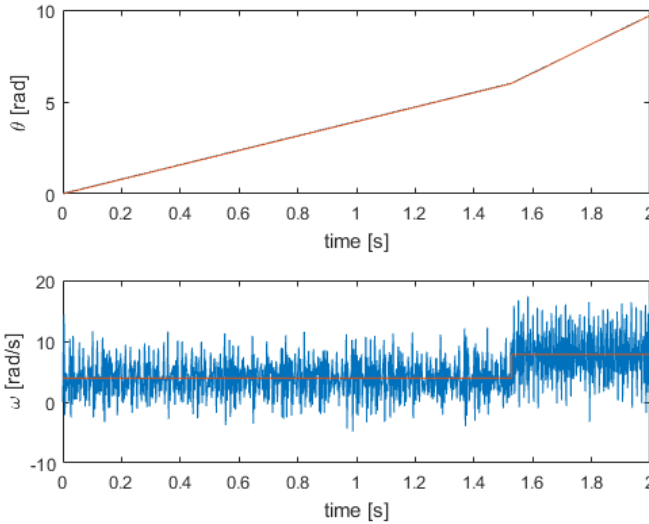


**Figure 8.1:** Simulation result when the parameters  $T_{dm} = 0.2152Nm$ ,  $B = 0.01186Nms/rad$  and  $\psi_m = -0.002854Vs/rad$  are used. The red curve represent the precalculated  $\theta$  and  $\omega$  and the blue is the results from the simulations.

## 8.2 Evaluation of the EKF

In this master thesis the EKF is used to estimate the states,  $\theta$ ,  $\omega$ ,  $i_a$  and  $i_b$ . Of most interest is  $\theta$ ,  $\omega$  because this parameters can be used in a future control algorithm to determine if the rotor follows the speed reference. They can also be used to obtain knowledge of the length the robot has traveled. Due to the result of the model and parameter determination described in Section 8.1 the parameters used in the EKF estimate are  $T_{dm} = 0.2152Nm$ ,  $B = 0.01186Nms/rad$  and  $\psi_m = -0.002854Vs/rad$ . As mentioned in Section 8.1 the model is developed to be used in the EKF and therefore the results presented in this section is essential to determine if the model is good enough or if the model needs to be modified.

To be able to test the performance of the EKF different datasets are tested and the histograms and ACF of the corresponding residuals are analysed. Two of the datasets used to evaluate the EKF are dataset 26 and 15 see Chapter 4.2. Dataset 26 is a dataset where the motor is run at a constant velocity, 3.927 rad/s and is chosen to show the properties of the EKF in a situation where the robot is run at constant velocity on a flat surface. Dataset 15 is a dataset which makes the motor take a step in velocity from 3.975 to 7.85 rad/s and is chosen to show how the EKF will perform in a more complex situation. Other datasets were tested but showed similar results and are therefore not presented in this report.

The result of the estimations from data 26 can be seen in Figure 8.5. It can be seen that the estimated states follows the precalculated values well. In Figure

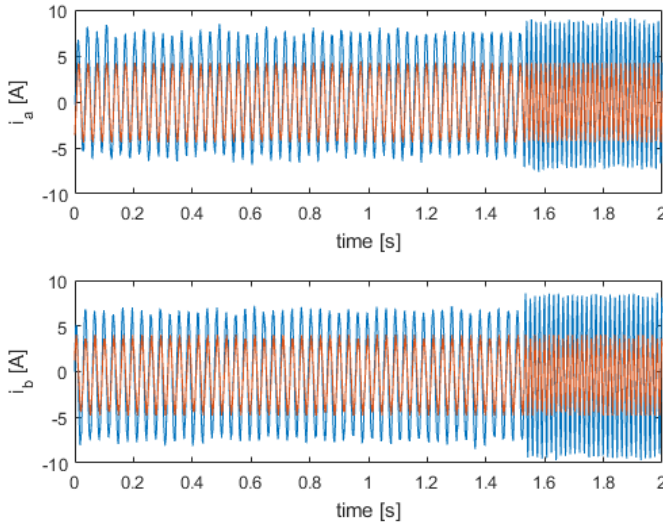


**Figure 8.2:** Simulation result when the parameters  $T_{dm} = 0.2152Nm$ ,  $B = 0.01186Nms/rad$  and  $\psi_m = -0.002854Vs/rad$  are used. The red curve is the measured current and the blue is the results from the simulations.

8.5 the histograms of the corresponding residuals are plotted. Here it can be seen that the result has a very small or none bias. The distribution of the current is close to normal distribution. The ACF of the residual is shown in Figure 8.7. The residuals for the angle  $\theta$  and angular velocity  $\omega$  are somewhat correlated. The ACF of the residuals for the phase current shows no correlation. The current estimates are better than the estimates of the angle and angular velocity because the current is the measured signal.

The result of the estimations from dataset 15 can be seen in Figure 8.8. The histogram and ACF for the corresponding residuals are shown in Figure 8.9 and 8.10. From the result it can be seen that the estimations of the rotor angle follows the precalculated value well. The estimates of the angular velocity is good until the angular velocity changes. After the change the variance of the angular velocity increases, however the mean of the angular velocity follows the theoretical value.

### 8.3 Evaluation of load angle estimations

The results from the EKF can first and foremost be used for speed control. Of interest is also to implement a torque control. This is of high interest since the produced torque depends on the applied current; an increase of current means an increase of the produced torque. Since the HSM is thought to be implemented in an application operated on batteries it is preferable for the motors to run with

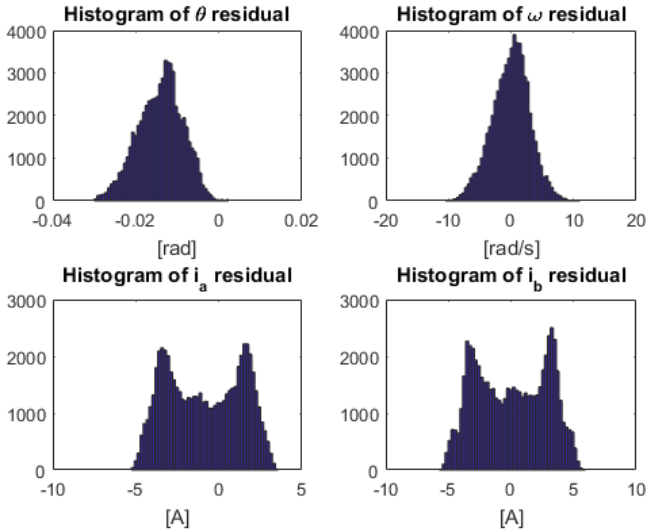


**Figure 8.3:** Histograms of the residuals when the parameters  $T_{dm} = 0.2152Nm$ ,  $B = 0.01186Nm/s/rad$  and  $\psi_m = -0.002854Vs/rad$  are used.

as low power as possible. However if the current is too low it is possible that the motor will loose steps. If step loss occurs it is possible that the estimates of the rotor angle will be incorrect. The step loss also causes unwanted noise and vibrations. To be able to gain information about the load and also to prevent step loss the load angle estimate is a good complement. In Chapter 3.2 it was mentioned that the relation between the load angle and the load torque should be sinusoidal. In Figure 8.11 it is possible to see the relations between the load angle and load torque for rotor angular velocity 3.927 rad/s and at maximum rated current, 1.8 Amp. It can be seen in the figure that the appearance of the curve is sinusoidal. At 3 Nm the motor will be stalled. In Figure 8.12 it can be seen how the load angle can vary when the rotor is completely stalled for one second. The fact that the rotor is stalled at 3 Nm is due to the holding torque, which is 3 Nm, see Table 4.2.

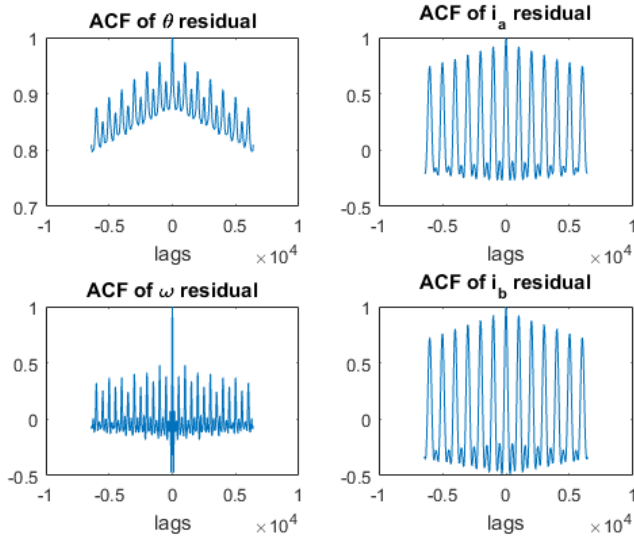


**Figure 8.4:** ACF of the residuals when the parameters  $T_{dm} = 0.2152Nm$ ,  $B = 0.01186Nms/rad$  and  $\psi_m = -0.002854Vs/rad$  are used.

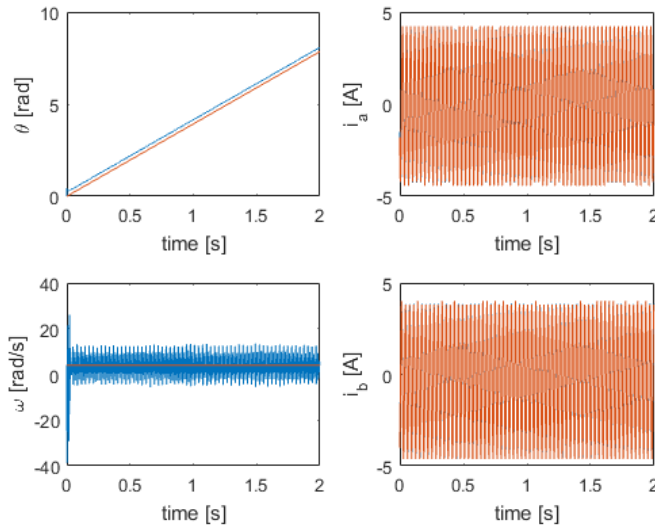


**Figure 8.5:** States estimated by the EKF for data 26 when the parameters  $T_{dm} = 0.2152Nm$ ,  $B = 0.01186Nms/rad$  and  $\psi_m = -0.002854Vs/rad$  were used. The red lines represents the expecting movement and the blue lines represent the estimated movement.

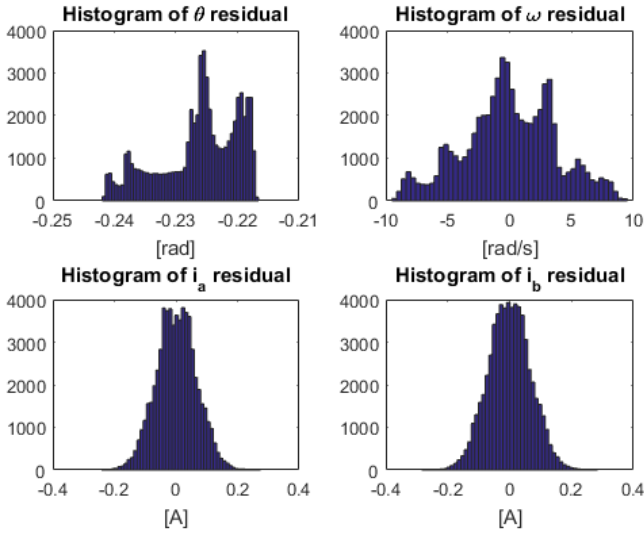


**Figure 8.6:** Histograms of the residuals calculated from the states estimated by the EKF for data 26 when the parameters  $T_{dm} = 0.2152Nm$ ,  $B = 0.01186Nm/s/rad$  and  $\psi_m = -0.002854Vs/rad$  were used.

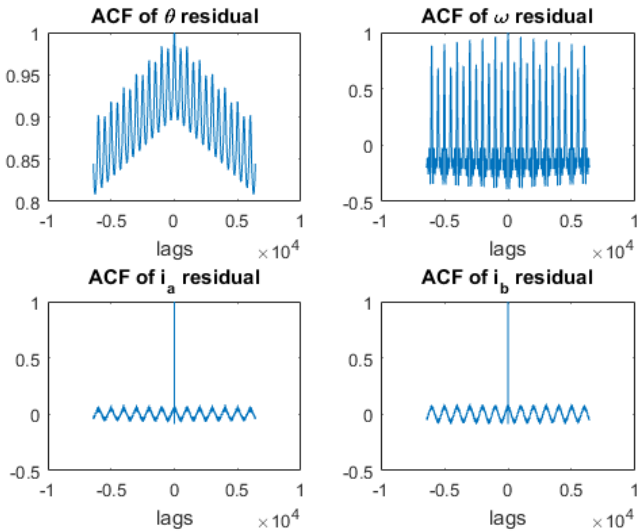


**Figure 8.7:** ACF of the residuals calculated from the states estimated by the EKF for data 26 when the parameters  $T_{dm} = 0.2152Nm$ ,  $B = 0.01186Nm/s/rad$  and  $\psi_m = -0.002854Vs/rad$  were used.

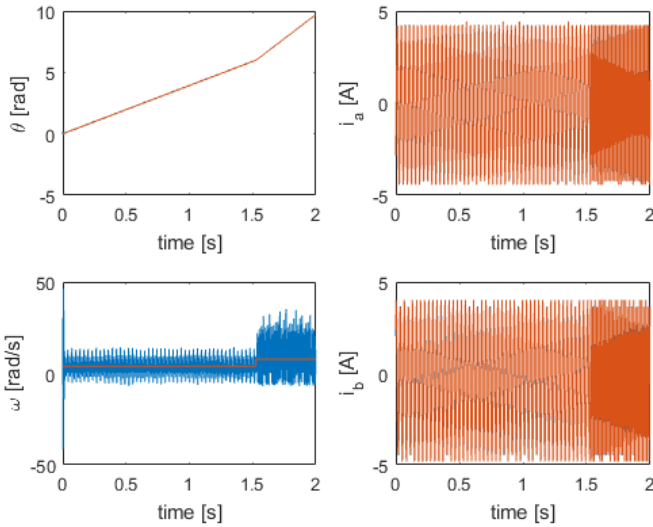


**Figure 8.8:** States estimated by the EKF for data 15 when the parameters  $T_{dm} = 0.2152Nm$ ,  $B = 0.01186Nm/s/rad$  and  $\psi_m = -0.002854Vs/rad$  were used. The red lines represents the expecting movement and the blue lines represent the estimated movement.

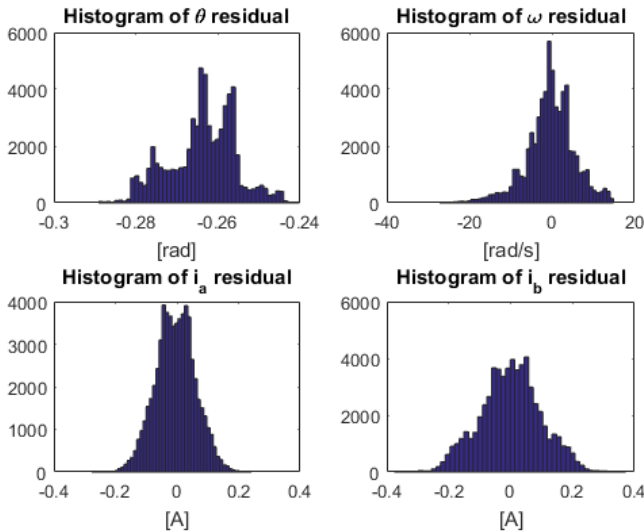


**Figure 8.9:** Histograms of the residuals calculated form the states estimated by the EKF for data 15 when the parameters  $T_{dm} = 0.2152Nm$ ,  $B = 0.01186Nm/s/rad$  and  $\psi_m = -0.002854Vs/rad$  were used.

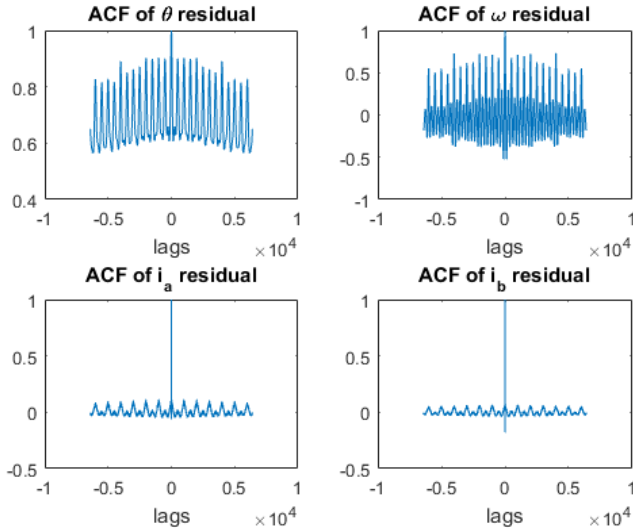


**Figure 8.10:** ACF of the residuals calculated from the states estimated by the EKF for data 15 when the parameters  $T_{dm} = 0.2152Nm$ ,  $B = 0.01186Nm/s/rad$  and  $\psi_m = -0.002854Vs/rad$  were used.

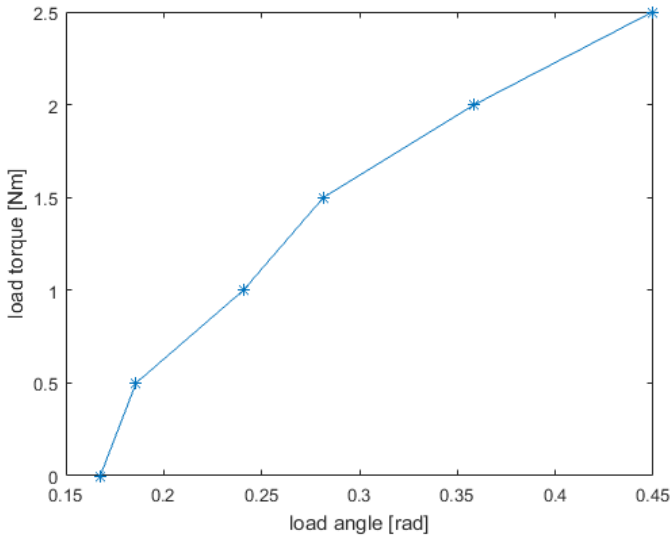


**Figure 8.11:** The relation between the load torque and load angle for  $\omega = 3.927 rad/s$

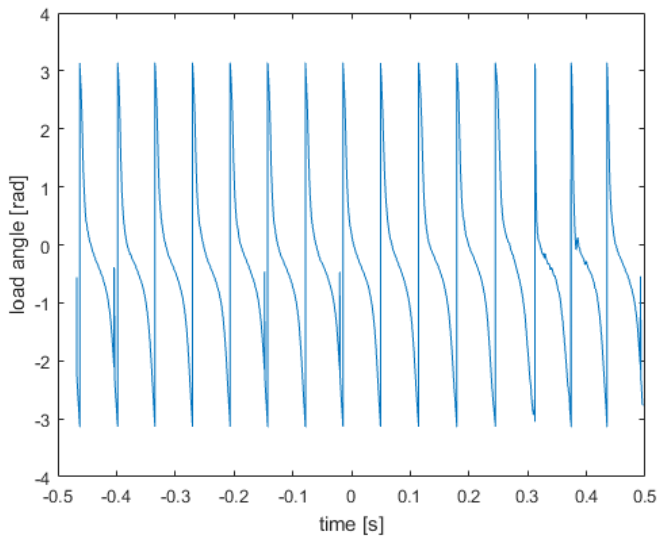


**Figure 8.12:** The appearance of the load angle when the motor is completely stalled.



# 9

---

## Discussion

In this chapter the results presented in Chapter 8 will be discussed. First a discussion of the parameter determination will be done and it will be followed with a discussion about the model. After that, the EKF and load angle estimate will be discussed. Finally the chapter will present how the results from this thesis can be used in the future.

### 9.1 Results

In this section the results presented in Chapter 8 will be discussed. First the modeling and parameter estimation will be discussed and after that follows a discussion about the EKF and load angle estimation.

#### 9.1.1 Motor model and parameters

The parameter estimation was not straight forward. Different methods, such as linear regression for one parameter at a time, multiple linear regression for all parameters and EKF have been used, and all of them gave different parameter sets. Residual analysis was used to determine which parameter set gave best result. Due to the lack of a positioning sensor, only theoretical values for the angle  $\theta$  and angular velocity  $\omega$ , could be compared with the estimated results. The precalculated values for the angular velocity  $\omega$  was a constant value. This is true for the real system in a way that at least the mean of the actual velocity has that value. Apart from this mean value it was impossible to know if the variations in the estimated velocities were in accordance with the system. This made the parameter determination difficult since several parameters gave similar results, and a positioning sensor had been helpful.

One observation of the results is that the estimations of the rotor angle often gives small constant biases. One explanation for this could be that the datasets are collected when the motor is rotating at a constant velocity and then when the dataset is used in a simulation the model starts at velocity zero. It is a possibility that there is an internal inertia in the model to overcome before the modelled motor can rotate as expected and this may create the biases seen in the results.

The model used in this thesis is a model based on basic electrical and mechanical equations. All system properties are not covered with the chosen model. One example is that the electrical equations neglects the position and current dependence of the magnetic flux linkage and inductance. It is possible that the results would have been closer to the reference system if this dependence would have been added in the model. However, this would have increased the complexity and made all calculations more time consuming. A too complex model could also make estimations worse. In this thesis, focus was on creating a model to an estimator, which in the future should be possible to implement in a robot. Therefore the less complex model was preferable. Also the fact that authors in [2], [14] and [15] presented good result with the basic model made it natural to implement that model.

### 9.1.2 EKF and load angle

The results from the EKF estimations showed good results. This provides that the model was a good choice. In the estimated velocity it is possible to see a noisy variation. As mentioned earlier this variation could be explained by the motor design. Because the motor takes steps by exiting its motor phases, the motion will not be completely smooth. However, without a positioning sensor it is not possible to say exactly how realistic these shown variations are, just that it is likely that some variations will exist.

The result of the load angle estimate seems promising. The relation between the load torque and load angle shows the sinusoidal appearance as expected. However it was also expected that the load angle would be zero when the load torque was zero. As seen in the results the load angle is around 0.17 when the load torque is zero. The reason for this could be that the internal rotor torque, such as the detent torque or the torque produced due to friction, also affects the load angle.

When the motor is completely stalled the load angle varies rapidly. This is reasonable since a stall makes the rotor stop in one position fixing the back EMF vector. Meanwhile the current vector rotates with the excitation changes in the phases and therefore the load angle will change.

All implementation and calculations done in this master thesis are performed with collected data with a very high sample time, almost 30 kHz. In a future implementation it is not possible to sample data this fast. The reason for why the data were collected with this sample rate were because the phase voltage changed very rapidly and when designing the model it was of interest to capture all model properties.

## 9.2 Future work

Since the EKF and the load angle has shown promising result it would be very interesting to take the evaluation of the hybrid stepper motor to the next level. This chapter will present suggestions for future work that can be done in the area.

The first thing to investigate is how the estimated data will change if the sample frequency changes. To sample the phase current at a lower rate should not be a problem. However problems could occur when it comes to the rapidly changing phase voltage.

### 9.2.1 Parameter determination

As mentioned in the previous discussion it was hard to distinguish different datasets from each other. In the report the prediction error is studied together with residual analysis. Another method to distinguish datasets with similar biases is to look at the root mean square, RMS, which is a measure of the variation. The RMS may give other datasets with better performance.

For determining the friction constant B, an assumption was made that the velocity decreases linearly to zero. Further it was discussed that this assumption may be incorrect and therefore an approach where the velocity were assumed to decrease exponential were tested. In the report a conclusion were made that there were to many unknown signals to be able to determine B. However, when the rotor rotates it creates an induced voltage which affects the phase voltage of the system. When the power of the system is cut the measured phase voltage is assumed to be the induced voltage. Because of this, an assumption could made that the relation between the rotor angular velocity and the phase voltage is

$$\omega \propto V \quad (9.1)$$

Equation (6.3) can therefore be rewritten as

$$V = V(0) \exp\left(-\frac{B}{J}t\right) \quad (9.2)$$

To determine B linear regression can be used where

$$Y = \ln\left(\frac{V}{V(0)}\right) \quad (9.3)$$

and

$$X = \frac{t}{J} \quad (9.4)$$

By using a dataset of the phase voltage when the power is cut and the motor decelerates it is possible to determine B. Maybe this method can be used to determine a better data set.

### 9.2.2 Extended Kalman Filter

In the EKF today, the load torque is seen as an unknown disturbance. However it could be of interest to estimate the load torque as well. To make this possible a model of the load torque needs to be developed. Since the robot shall be able to operate in very varying areas it could be difficult to create a model that covers all variations. However authors in [14] states that even a simple model of the load torque can provide good estimates and the area would therefore be interesting to investigate.

### 9.2.3 Load angle

To determine the load angle a test bench for breaking the motor was used. With this equipment it was possible to increase the load torque and observe how the load angle changed. The information given from the load angle can be used to control the applied current when the robot reaches an uphill or an obstacle. To be able to do an accurate current control it is also important to know how the load angle is affected when the robot reaches a downhill, and the load torque is negative. To be able to investigate this an experiment can be made where the motor is pushed by another motor.

The load angle varies when there is a change in load torque or current. This is because a change in the current changes the produced torque. Also the velocity can affect the load angle since a higher velocity reduces the produced torque. In order to utilize all information in the load angle it could be of high interest to investigate how the relationship between the load angle and the load torque changes for different velocities and currents.

When the behaviour of the load angle is known it can be used for stall detection. The most simple way is to implement a threshold function as adapts with the rotor speed and the applied load torque. This implementation can for example be used to detect collisions.

# 10

---

## Conclusions

This master thesis has investigated the possibilities to replace a BLDC-motor and a gearbox with a hybrid stepper motor. The main goal was to develop a possible estimator for estimating information about the motor that could be used in a future speed and torque control algorithm.

This thesis work has been treating modelling and estimations of a hybrid stepper motor. For modelling fundamental electrical and mechanical equations were used. Decisions were made that a model based on these equations will be able to describe the needed system behaviour and therefore an extended model were not developed. It is advantageous to use the basic model in a future implementation because it will be less time consuming as a more complex model. A major problem with the modelling has been the lack of a positioning sensor. This made it difficult to determine which parameter set that best described the real system. There is a possibility that other parameter sets can describe the system better.

For estimations of the rotor angle and angular velocity an EKF has been tested. The EKF is used because it allows the model to be nonlinear. When tuned correctly the EKF gives good results of the estimations. Also here a problem occurred due to the lack of a positioning sensor because the data to compare with was not as accurate as might have been desirable.

As a complement to the EKF estimates the load angle was investigated. The relation between the load angle and the load torque would, according to authors in [7], be sinusoidal and that was also the result of the investigation in this thesis. For implementing the load angle estimation the sliding discrete fourier transform was used. This variant of the fourier transform makes it possible to update the load angle estimate in a more efficient way.

The goal of this master thesis was to investigate the possibility to develop a sensorless estimator to a Hybrid Stepper Motor. This to examine if it is possible to replace a BLDC-motor together with a gearbox with a Hybrid Stepper motor.

It was shown that an EKF which estimates the rotor angle and rotor angular velocity, together with a load angle estimate should be able to give enough feedback to a controller. The results of this thesis can be used as a basis for further investigations on the Hybrid Stepper motor. This to decide whether a stepper motor is a good alternative for propulsion of autonomous lawn mowing robots.

---

## Bibliography

- [1] P. P. Acarnley. *Stepping motors : a guide to theory and practice, fourth edition. [Elektronisk resurs].* IEE control engineering series: 63. London : Institution of Electrical Engineers, c2002. ISBN 0852960298. Cited on pages 7 and 8.
- [2] M. Bendjedia, Y. Ait-Amirat, B. Walther, and A. Berthon. Position control of a sensorless stepper motor. *IEEE Transactions on Power Electronics*, 27(2):578–587, Feb 2012. ISSN 0885-8993. doi: 10.1109/TPEL.2011.2161774. Cited on pages 5, 6, and 60.
- [3] S. Bolognani, L. Tubiana, and M. Zigliotto. Extended kalman filter tuning in sensorless pmsm drives. *IEEE Transactions on Industry Applications*, 39(6):1741–1747, Nov 2003. ISSN 0093-9994. doi: 10.1109/TIA.2003.818991. Cited on page 37.
- [4] M. Butcher, A. Masi, R. Picatoste, and A. Giustiniani. Hybrid stepper motor electrical model extensions for use in intelligent drives. *IEEE Transactions on Industrial Electronics*, 61(2):917–929, Feb 2014. ISSN 0278-0046. doi: 10.1109/TIE.2013.2254097. Cited on pages 5 and 6.
- [5] S. Derammelaere, L. Carlier, B. Vervisch, C. Debruyne, K. Stockman, L. Vandeveldel, P. Cox, and G. Van den Abeele. The opportunities of two-phase hybrid stepping motor back emf sampling. In *2011 IEEE Energy Conversion Congress and Exposition*, Technical University College of West-Flanders, Kortrijk, Belgium, . Cited on page 6.
- [6] S. Derammelaere, C. Debruyne, F. D. Belie, K. Stockman, and L. Vandeveldel. Load angle estimation for two-phase hybrid stepping motors. *IET Electric Power Applications*, 8(7):257–266, August 2014. ISSN 1751-8660. doi: 10.1049/iet-epa.2013.0333. Cited on pages 6 and 11.
- [7] Stijn Derammelaere, Colin Debruyne, Frederik De Belie, Kurt Stockman, and Lieven Vandeveldel. Load angle estimation for two-phase hybrid stepping motors. *IET Electric Power Applications*, 8(7):257 – 266, . ISSN 17518660. doi: 10.1049/iet-epa.2013.0333. Cited on pages 5, 6, 10, 11, 46, 47, and 63.

- [8] Mille Millnert Fredrik Gustafsson, Lennart Ljung. *Signal Processing*. Studentlitteratur, 1:3 edition, 2010. ISBN 978-91-44-05835-1. Cited on page 13.
- [9] Fredrik Gustafsson. *Statistical Sensor Fusion*. Studentlitteratur, 2:1 edition, 2012. ISBN 978-91-44-07732-1. Cited on page 13.
- [10] T. A. Khan, T. A. Taj, and I. Ijaz. Hybrid stepper motor and its controlling techniques a survey. In *Electrical and Electronic Engineering Conference (EIConRusNW), Proceedings of the 2014 IEEE NW Russia Young Researchers in*, pages 79–83, Feb 2014. doi: 10.1109/EIConRusNW.2014.6839207. Cited on page 5.
- [11] Torkel Glad Lennart Ljung. *Modellbygge och simulering*. Studentlitteratur, 2:5 edition, 2004. ISBN 978-91-44-02443-1. Cited on page 12.
- [12] Bertil Westergren Lennart Råde. *Mathematics Handbook, for Scinece and Engineering*. Studentlitteratur, 5:12 edition, 2004. ISBN 978-91-44-03109-5. Cited on page 13.
- [13] Allegro MicroSystems LLC. *Dual Full-Bridge MOSFET Driver with Microstepping Translator*. Cited on page 15.
- [14] J. Persson and Y. Perriard. An optimized extended kalman filter algorithm for hybrid stepper motors. In *Industrial Electronics Society, 2003. IECON '03. The 29th Annual Conference of the IEEE*, volume 1, pages 297–300 vol.1, Nov 2003. doi: 10.1109/IECON.2003.1279995. Cited on pages 5, 6, 60, and 62.
- [15] D. Samokhvalov, S. Stoliarov, and A. Kekkonen. The hybrid stepper motor modeling in simulink. In *Young Researchers in Electrical and Electronic Engineering Conference (EIConRusNW), 2015 IEEE NW Russia*, pages 282–285, Feb 2015. doi: 10.1109/EIConRusNW.2015.7102280. Cited on pages 5, 6, 23, 25, and 60.
- [16] Stephen D. Umans. *Fitzgerald & Kingsley's Electric Machinery*. McGraw-Hill Education, seventh international edition edition, 2014. ISBN 978-1-259-25466-6. Cited on pages 5 and 7.
- [17] Sanford Weisberg. *Applied linear regression. [Elektronisk resurs]*. Wiley Series in Probability and Statistics. Hoboken, New Jersey : Wiley, 2014., 2014. ISBN 9781118386088. Cited on page 12.